Advances in Nano Research, *Vol. 17, No.2 (2024) 181-195*
https://doi.org/10.12989/anr.2024.17.2.181

Size-dependent free vibration of coated functionally graded graphene reinforced nanoplates rested on viscoelastic medium

Ali Alnujaie[1,2], Ahmed A. Daikh*[3,4], Mofareh H. Ghazwani[1,2], Amr E. Assie[1,6] and Mohamed A Eltaher[5,6]

[1]*Department of Mechanical Engineering, College of Engineering and Computer Sciences, Jazan University, P.O Box 45124, Jazan, Saudi Arabia*
[2]*Engineering and Technology Research Center, P.O. Box 114, Jazan 82817, Saudi Arabia*
[3]*Artificial Intelligence Laboratory for Mechanical and Civil Structures and Soil, University Centre of Naama, P.O. Box 66, Naama 45000, Algeria*
[4]*Laboratoire d'Etude des Structures et de Mécanique des Matériaux, Département de Génie Civil, Faculté des Sciences et de la Technologie, Université Mustapha Stambouli B.P. 305, R.P.29000 Mascara, Algérie*
[5]*Mechanical Engineering Department, Faculty of Engineering, King Abdulaziz University, P.O. Box 80204, Jeddah 21589, Saudi Arabia*
[6]*Mechanical Design & Production Department, Faculty of Engineering, Zagazig University, Zagazig 44519, Egypt*

(*Received April 6, 2023, Revised July 29, 2024, Accepted August 11, 2024*)

Abstract. This study introduces a novel functionally graded material model, termed the "Coated Functionally Graded Graphene-Reinforced Composite (FG GRC)" model, for investigating the free vibration response of plates, highlighting its potential to advance the understanding and application of material property variations in structural engineering. Two types of coated FG GRC plates are examined: Hardcore and Softcore, and five distribution patterns are proposed, namely FG-A, FG-B, FG-C, FG-D, and FG-E. A modified displacement field is proposed based on the higher-order shear deformation theory, effectively reducing the number of variables from five to four while accurately accounting for shear deformation effects. To solve the equations of motion, an analytical solution based on the Galerkin approach was developed for FG GRC plates resting on a viscoelastic Winkler/Pasternak foundation, applicable to various boundary conditions. A comprehensive parametric analysis elucidates the impact of multiple factors on the fundamental frequencies. These factors encompass the types and distribution patterns of the coated FG GRC plates, gradient material distribution, porosities, nonlocal length scale parameter, gradient material scale parameter, nanoplate geometry, and variations in the elastic foundation. Our theoretical research aims to overcome the inherent challenges in modeling structures, providing a robust alternative to experimental analyses of the mechanical behavior of complex structures.

Keywords: coated nanoplates; four variable higher-order shear deformation theory; nonlocal strain gradient theory; vibration response; viscoelastic foundation

1. Introduction

Functionally graded materials (FGMs) are a new type of composite materials that have a gradual change in constituents throughout spatial directions. The purpose of FGMs is to reduce the sudden concentration of stress between different layers and to be used as a thermal barrier in aircraft, submarines, space station structures, and fusion reactors. FGMs have several improved properties, including higher fracture toughness, improved stress spreading, enhanced thermal resistance, and lower stress intensity factors. These materials have now been developed for general use in various fields of engineering.

Graphene has remarkable physical, thermal, and mechanical properties, making it an attractive choice for use in functionally graded graphene-reinforced nanocomposites (FG-GRCs). These materials have excellent reinforcing nano-fillers, better dispersion, and relatively low manufacturing costs. As a result, many studies have started to focus on the use of graphene in FG-GRCs. Chen *et al*. (2017) used Timoshenko beam theory and mid-plane stretching to predict the postbuckling and nonlinear vibration of multilayer FG-GRCs, including the effect of porosity. On the other hand, Shen *et al*. (2017a, b) developed models and analyzed the thermal bending and postbuckling behavior of GRC laminated plates resting on an elastic foundation and subjected to in-plane temperature variations. Huang *et al*. (2018) conducted a study on the nonlinear buckling analysis of FG-GRC shallow arches with elastic rotational constraints under uniform radial loads. Meanwhile, Song *et al*. (2018) performed bending and buckling analyses of multilayer FG-GRC polymer composite plates using the first-order shear deformation theory "FSDT". The effective Young's modulus of the nanocomposites was estimated through the Halpin-Tsai micromechanics model. Garcia-Macias *et al*. (2018) used a two-parameter agglomeration model to estimate the agglomeration effects of carbon nanotubes (CNTs) as reinforcement in composite structures. They also studied the effects of restacking graphene sheets on the bending and free-vibration behaviors of composite plates. Dong *et al*. (2018) investigated the buckling behavior of FG-GRC porous cylindrical plates with

*Corresponding author, Professor,
E-mail: daikhresearch@gmail.com

ISSN: 2287-237X (Print), 2287-2388 (Online)

spinning motion subjected to external axial compressive forces and radial pressures using the FSDT. Daikh and Megueni (2018) studied the influences of plate aspect ratio, gradient index, and thermal loading conditions on the critical buckling of functionally graded material (FGM) sandwich plates modeled using the higher-order shear deformation plate theory "HSDT". Liu *et al*. (2018&2019) studied the bending, buckling, and vibration behaviors of initially stressed functionally graded (FG) cylindrical plates and circular plates reinforced with nonuniformly distributed graphene platelets (GPLs) using the state-space formulation. Polit *et al*. (2019) presented the impacts of different dispersion patterns for the graphene and porosity, shallowness of the curved beam, thickness ratio, and platelet geometry on the bending and elastic stability of a higher-order beam with nonlinear stretching. Yang *et al*. (2019) investigated the nonlinear in-plane buckling of fixed shallow FG-GRC arches subjected to uniform radial loads and temperature fields. Mao and Zhang (2019) analyzed the effects of electric potential and axial forces on the buckling and postbuckling behavior of piezoelectric FG-GRC. Anirudh *et al*. (2019) employed a trigonometric shear deformation theory and finite element method to investigate the mechanical response of curved beams made of porous FG-GRC. Tam *et al*. (2019, 2020) used the finite element method to study the nonlinear bending, free vibration, and buckling properties of FG-GRC beams that had open edge cracks. Thai *et al*. (2019, 2020) investigated the mechanical properties of multilayer FG-GRC plates using the four-variable refined plate theory and modified couple stress theory. Zhao *et al*. (2020) provided a detailed review on FG-GRC structures, including their mechanical properties, micromechanics models, technical challenges, and future research directions. Eltaher *et al*. (2020b) used the finite element method to investigate the elastic and elastoplastic indentation responses of FGMs with frictional contact mechanics. Rahimi *et al*. (2020) analyzed the bending and vibration behavior of a cylindrical GRC plate using the state space technique. To summarize, Shahgholian *et al*. (2020) investigated the buckling of a porous cylindrical FG-GRC plate using the FSDT. On the other hand, Hamed *et al*. (2020a, b) analyzed the effect of varying in-plane compressive forces on the critical buckling loads and buckling modes of composite laminated and FG porous sandwich beams that are resting on an elastic foundation using a unified higher-order beam theory. Wang *et al*. (2020) studied the nonlinear bending behavior of FG-GRC plates with dielectric permittivity using the FSDT. Karami and Shahsavari (2020) investigated forced resonant vibration analysis of four different geometries of FG-GRC doubly curved nano-plates, namely, elliptical, hyperbolic, and cylindrical. They used the Halpin-Tsai model and a rule of mixture to estimate the effective material properties.

In recent years, there has been a growing recognition of the importance of micro- and nanoscale effects in determining the overall mechanical behavior of materials. The classical approach of continuum mechanics often neglects these effects, and mechanical properties are typically determined solely from macroscopic analysis. However, it is now widely recognized that micro- and nanoscale effects can significantly impact the mechanical behavior of materials, and continuous mechanics theories are being developed to account for these effects.

Sahmani *et al*. (2018) investigated the nonlinear bending behavior of porous FG-GRC nanobeam with consideration of size effect. The beam was subjected to uniform distributed load and axial compressive load, and the nonlocal strain gradient theory "NSGT" of elasticity was utilized in the analysis. Emam *et al*. (2018) analytically investigated the postbuckling and vibration response of curved multilayer nanobeams subjected to a pre-stress compressive load. Nonlocal elasticity was used in the analysis. Brahimi and Barati (2018) investigated the impact of hygro-thermal effects and size-scale on the vibration response of graphene sheets supported on a viscoelastic medium, using the NSGT. Daikh *et al*. (2019) used NSGT to analyze the thermal buckling behavior of porous FG sandwich nanoplates on a Kerr foundation. Fattahi *et al*. (2019) created a beam model that utilized NSGT and the Galerkin technique with multiple timescales to forecast the nonlinear secondary resonance of FG porous micro/ nanobeams subjected to periodic excitation. Karami *et al*. (2019) investigated the static bending behavior of FG nanoplates made of hexagonal beryllium crystals with anisotropic properties using NSGT. Jalaei and Civalek (2019) used NSGT to investigate the thermal effects on the dynamic instability of a graphene sheet subjected to periodic axial load. Daikh *et al*. (2020a) proposed a comprehensive model using nonlocal strain gradient constitutive relation to analyze the bending behavior of cross-ply carbon nanotubes reinforced composite (CNTRC) laminated nanobeams under different loading conditions. Ebrahimi and Dabbagh (2020) investigated viscoelastic wave propagation in axially loaded double-layered graphene sheets using NSGT. Eltaher and Mohamed (2020) and Eltaher *et al*. (2020a) studied the size-scale effect of CNT beam structures on buckling stability and free vibration using doublet mechanics theory. Mohamed *et al*. (2020) used the energy-equivalent method to analyze the size scale effect on the buckling and post-buckling behavior of single-walled carbon nanotubes resting on nonlinear elastic foundations. Daikh and Zenkour (2020) introduced an improved NSGT to predict the stresses and deflections of FG sandwich nanoplates supported by a Pasternak elastic foundation. Using nonlocal elasticity, Daikh *et al*. (2020b) analytically investigated the vibration behavior of FG sandwich nanoplates under thermal conditions using an HSDT. Torabi *et al*. (2020) investigated the dynamic and pull-in instability of FG nanoplates using NSGT and the homotopy method as an analytical solution technique. Xiao and Dai (2020) analyzed the static behavior of circular nanotubes made of FG materials using NSGT and a refined shear model. Dastjerdi *et al*. (2021) developed a semi-analytical solution to study the bending behavior of moderately thick FGM plates in a hygro-thermal environment using a quasi-3D approach with nonlocal constitutive equations. Abo-bakr *et al*. (2020) used the Pareto optimality method to obtain the optimal weight for maximum buckling of an FG beam under variable axial load.

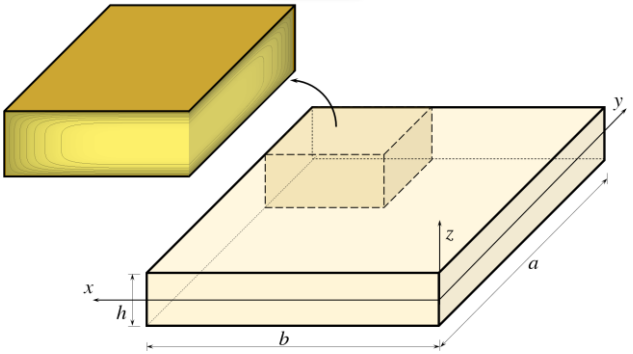

Fig. 1 Tri-coated FG GRC plate geometry

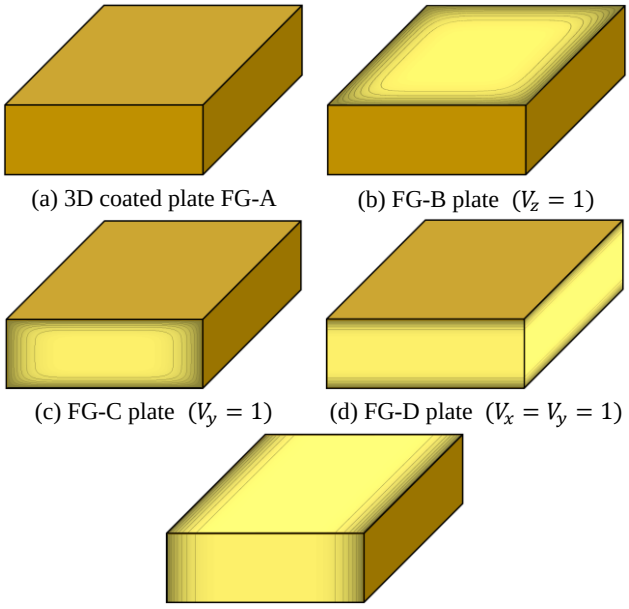

(a) 3D coated plate FG-A (b) FG-B plate $(V_z = 1)$

(c) FG-C plate $(V_y = 1)$ (d) FG-D plate $(V_x = V_y = 1)$

(e) FG-E plate $(V_y = V_z = 1)$

Fig. 2 Various schemes of Tri- and Bi-coated FG GRC plate

The aim of this research is to conduct a comprehensive investigation into the free vibration of composite plates reinforced with graphene. Specifically, the focus is on the coated functionally graded (FG) graphene-reinforced composite (GRC), considering five different distribution patterns of graphene platelets (GPLs). The proposed solution is limited only to plates with uniform thicknesses and opposite boundary conditions (e.g., SSSS, CCCC, CCSS). The study is divided into several sections. In Section 2, the material distribution and graduation functions are presented using the Halpin-Tsai model. Sections 3 outline the governing equations based on the generalized shear deformation plate theory. Section 4 covers the analytical solutions and admissible boundary conditions. The model verification and numerical parametric studies are discussed in Section 5. Finally, Section 6 summarizes the conclusions and main points of the study.

2. Material properties

The structure being studied is a composite plate with length *a*, width *b*, and thickness *h* (See Fig. 1). The plate's midplane has principal curvature radii R_x and R_y in the x and y directions, respectively. The plate is composed of an epoxy matrix reinforced with graphene nanoplatelets (GPLs), with the weight fraction of GPLs varying in the three directions of the plate. Two types of FG GRC plates are presented: hardcore FG plates and softcore FG plates. Five patterns of GPLs distribution are considered: FG-A GRC (tridirectionally material distribution pattern), FG-B GRC and FG-C GRC (two bidirectional material distribution patterns), FG-D GRC (unidirectional transverse material distribution), and FG-E GRC (unidirectional axial material distribution) as shown in Fig. 2.

The law of mixture is a widely used method for calculating the overall properties of composite materials. It states that the properties of a composite material, such as Young's modulus, mass density, and Poisson's ratio, can be determined by considering the properties of the individual components and their volume fractions in the mixture. This method is applicable to both isotropic and anisotropic composite materials.

$$P(x,y,z) = P_m + (P_e - P_m)V(x,y,z) \tag{1}$$

In the above equation, P_m and P_e represent the mechanical properties of the matrix and the effective material properties of the matrix/GPL constituents, respectively.

The volume fraction $V(x,y,z)$ which is related only to the rectangular sections of the matrix/graphene platelet (GPL) phase in the x, y, and z directions, is determined by three functions, denoted as $V(x)$, $V(y)$, and $V(z)$, which represent the distribution of GPLs in the plate along these directions.

$$\begin{cases} V(x) = \left[\left(\dfrac{|2x-a|}{a}\right)^k - 1\right] \\ V(y) = \left[\left(\dfrac{|2y-b|}{b}\right)^k - 1\right] \\ V(z) = \left[\left(\dfrac{|2z|}{h}\right)^p - 1\right] \end{cases} \tag{2}$$

The total volume fraction $V(x,y,z)$ of the Hardcore (HC) coated FG-GRC plate can be expressed as:

$$V(x,y,z) = V(x)V(y)V(z) \tag{3}$$

And for the Softcore (SC) coated FG-GRC plate:

$$V(x,y,z) = 1 - V(x)V(y)V(z) \tag{4}$$

The Halpin-Tsai model is a commonly used model to predict the effective mechanical properties of composite materials reinforced by nanoparticles, such as graphene. The model assumes that the reinforcing particles are uniformly distributed throughout the matrix material and aligned parallel to the plate axis. It also assumes that the reinforcing particles are much stiffer than the matrix material and that their distribution is isotropic.

$$E_e = \frac{3}{8}\frac{1+\xi_L\eta_L V_{GPL}}{1-\eta_L V_{GPL}}E_m + \frac{5}{8}\frac{1+\xi_W\eta_W V_{GPL}}{1-\eta_W V_{GPL}}E_m \tag{5}$$

where

$$\eta_{\mathrm{L}}=\frac{(E_{\mathrm{GPL}}/E_m)-1}{(E_{\mathrm{GPL}}/E_m)+\xi_{\mathrm{L}}} \tag{6}$$

$$\eta_{\mathrm{W}}=\frac{(E_{\mathrm{GPL}}/E_m)-1}{(E_{\mathrm{GPL}}/E_m)+\xi_{\mathrm{W}}} \tag{7}$$

$$\xi_{\mathrm{L}}=2\left(\frac{a_{\mathrm{GPL}}}{h_{\mathrm{GPL}}}\right) \tag{8}$$

$$\xi_{\mathrm{W}}=2\left(\frac{b_{\mathrm{GPL}}}{h_{\mathrm{GPL}}}\right) \tag{9}$$

The effective Poisson's ratio υ_{e} of the epoxy/GPL phase can be computed as follows:

$$\upsilon_{\mathrm{e}}=\upsilon_{\mathrm{GPL}}V_{GPL}+\upsilon_{\mathrm{m}}V_{\mathrm{m}} \tag{10}$$

υ_{GPL} and υ_{m} are Poisson's ratio of the GPLs and the matrix. V_{GPL} and V_m are the GPLs and the matrix volume fraction, respectively, where:

$$V_{GPL}=\frac{W_{GPL}}{W_{GPL}+(\rho_{\mathrm{GPL}}/\rho_{\mathrm{m}})(1-W_{\mathrm{GPL}})} \tag{11}$$

And

$$V_m=1-V_{GPL} \tag{12}$$

3. Mathematical formulations

3.1 Generalized shear deformation plate theory

Various plate theories have been developed and studied in the literature, including the classical plate theory (CPT), the FSDT) and the HSDT. The FSDT was proposed to address the limitation of the CPT, which neglected the impact of transverse shear strain. However, the HSDT was later introduced to account for zero shear at the plate's top and bottom surfaces. The displacement field for the generalized HSDT can be expressed as:

$$\begin{aligned} u(x,y,z,t)&=u_0-z\frac{\partial w_0}{\partial x}+f(z)\psi_x\\ v(x,y,z,t)&=v_0-z\frac{\partial w_0}{\partial y}+f(z)\psi_y\\ w(x,y,z,t)&=w_0 \end{aligned} \tag{13}$$

In which u, v and w are the displacements in the directions x, y and z, respectively, and ψ_x and ψ_y are the rotations. The shape function for the shear distribution can be given as

$$f(z)=h\sinh\left(\frac{z}{h}\right)-\frac{3z^3}{2h^2} \tag{14}$$

The present displacement model is based on assumptions that ensure the rotation angles ψ_x and ψ_y are equal ($\psi_x=\psi_y=\psi$). Specifically, the plate is assumed to have a uniform thickness, and the boundary conditions on opposite edges of the plate must be identical (see Fig. 2). As a result, the displacement field can be expressed as:

$$\begin{aligned} u(x,y,z,t)&=u_0-z\frac{\partial w_0}{\partial x}-f(z)\frac{\partial \psi}{\partial x}\\ v(x,y,z,t)&=v_0-z\frac{\partial w_0}{\partial y}-f(z)\frac{\partial \psi}{\partial y}\\ w(x,y,z,t)&=w_0 \end{aligned} \tag{15}$$

With the modified displacement field assumed in Eq. (15), the strains at any point within the nanoplate domain can be expressed as follows:

$$\begin{Bmatrix}\varepsilon_{xx}\\ \varepsilon_{yy}\\ \gamma_{xy}\\ \gamma_{yz}\\ \gamma_{xz}\end{Bmatrix} =\begin{bmatrix} u_{0,x} & -w_{0,xx} & \psi_{,xx} & 0 & 0\\ v_{0,y} & -w_{0,yy} & \psi_{,yy} & 0 & 0\\ v_{0,x} & -2w_{0,xy} & -2\psi_{,xy} & 0 & 0\\ 0 & 0 & 0 & \phi_{,y}-\psi_{,y} & 0\\ 0 & 0 & 0 & \phi_{,x}-\psi_{,x} & 0\end{bmatrix}\begin{Bmatrix}1\\ z\\ f(z)\\ f'(z)\\ f''(z)\end{Bmatrix} \tag{16}$$

Taking into consideration the contribution of strain gradient stress and nonlocal elastic stress, the constitutive equation governing the behavior of the nanoplate can be expressed as:

$$\sigma_{ij}=\sigma_{ij}^{(0)}-\frac{d\sigma_{ij}^{(1)}}{dx} \tag{17}$$

The stress tensor $\sigma_{ij}^{(0)}$ and the higher-order stress tensor $\sigma_{ij}^{(1)}$ depend on the strain tensor ε_{kl} and the first-order strain gradient tensor $\varepsilon_{kl,x}$, and can be expressed as:

$$\sigma_{ij}^{(0)}=\int_0^L C_{ijkl}\alpha_0(x,x',e_0a)\varepsilon_{kl}(x')\mathrm{d}x' \tag{18}$$

$$\sigma_{ij}^{(1)}=l^2\int_0^L C_{ijkl}\alpha_1(x,x',e_1a)\varepsilon_{kl,x}(x')\mathrm{d}x' \tag{19}$$

C_{ijkl} are elastic constants, l represents the material length scale parameter which distinct the field of the strain gradient stress. The nonlocal parameters which distinct the field of the nonlocal elastic stress are e_0a and e_1a, and $\alpha_0(x,x',e_0a)$ and $\alpha_1(x,x',e_1a)$ are the nonlocal kernel functions. The constitutive relation is given as

The constitutive relation of the nanoplate takes into account the effect of strain gradient stress and nonlocal elastic stress and can be expressed as:

$$\begin{aligned}&[1-(e_1a)^2\nabla^2][1-(e_0a)^2\nabla^2]\sigma_{ij}=\\ &C_{ijkl}[1-(e_1a)^2\nabla^2]\varepsilon_{kl}-C_{ijkl}l^2[1-(e_0a)^2\nabla^2]\nabla^2\varepsilon_{kl}\end{aligned} \tag{20}$$

where C_{ijkl} are the elastic constants, l is the material length scale parameter that characterizes the field of the strain gradient stress, e_0a and e_1a are the nonlocal parameters that distinguish the field of the nonlocal elastic stress, and $\alpha_0(x,x',e_0a)$ and $\alpha_1(x,x',e_1a)$ are the nonlocal kernel functions.

$\nabla^2=\frac{\partial^2}{\partial x^2}+\frac{\partial^2}{\partial y^2}$ describes the Laplacian operator. The strain gradient constitutive relations can be expressed as Eq.

(15) by assuming that the nonlocal parameters e_0 and e_1 are equal to the same value e. This can be written as:

$$[1-\mu\nabla^2]\sigma_{ij} = C_{ijkl}[1-\lambda\nabla^2]\varepsilon_{kl} \tag{21}$$

where $\mu = (ea)^2$ and $\lambda = l^2$.

The stress-strain relations for the nonlocal strain gradient constitutive model are given by:

$$\begin{Bmatrix} \sigma_{xx}-\mu\nabla^2\sigma_{xx} \\ \sigma_{yy}-\mu\nabla^2\sigma_{yy} \\ \tau_{yz}-\mu\nabla^2\tau_{yz} \\ \tau_{xz}-\mu\nabla^2\tau_{xz} \\ \tau_{xy}-\mu\nabla^2\tau_{xy} \end{Bmatrix} = \begin{bmatrix} Q_{11} & Q_{12} & 0 & 0 & 0 \\ Q_{12} & Q_{22} & 0 & 0 & 0 \\ 0 & 0 & Q_{44} & 0 & 0 \\ 0 & 0 & 0 & Q_{55} & 0 \\ 0 & 0 & 0 & 0 & Q_{66} \end{bmatrix} \begin{Bmatrix} \varepsilon_{xx}-\lambda\nabla^2\varepsilon_{xx} \\ \varepsilon_{yy}-\lambda\nabla^2\varepsilon_{yy} \\ \gamma_{yz}-\lambda\nabla^2\gamma_{yz} \\ \gamma_{xz}-\lambda\nabla^2\gamma_{xz} \\ \gamma_{xy}-\lambda\nabla^2\gamma_{xy} \end{Bmatrix} \tag{22}$$

where

$$\begin{gathered} Q_{11} = Q_{22} = \frac{E(x,y,z)}{1-\upsilon^2} \\ Q_{12} = \upsilon Q_{11} \\ Q_{44} = Q_{55} = Q_{66} = \frac{E(x,y,z)}{2(1+\upsilon)} \end{gathered} \tag{23}$$

3.2 Governing Equations

To obtain the governing equations, the principle of Hamilton is applied, which can be written as:

$$\delta\int_{t_2}^{t_1}\delta(U+F-T)dt = 0 \tag{24}$$

where δU, δF and δT are variations of the strain energy, elastic foundation and kinetic energy, respectively.

As the strain energy is a functional of the displacement field, the variation of the strain energy δU can be written as:

$$\delta U = \int_V \begin{bmatrix} \sigma_{xx}\delta\varepsilon_{xx}+\sigma_{yy}\delta\varepsilon_{yy} \\ +\tau_{xy}\gamma_{xy}+\tau_{yz}\gamma_{yz}+\tau_{xz}\gamma_{xz} \end{bmatrix} dV \tag{25}$$

The variation of the kinetic energy of the coated FG plate can be represented as δT.

$$\delta T = \frac{1}{2}\int_0^L\int_A \rho(\dot{u}\delta\dot{u}+\dot{v}\delta\dot{v}+\dot{w}\delta\dot{w})\,dAdx \tag{26}$$

The Viscoelastic/Winkler/Pasternak foundation can be defined as a collection of springs, dashpots, and viscous elements that are connected in parallel and extend infinitely.

$$\begin{gathered} \delta F = F_{\text{spring}} + F_{\text{shear}} + F_{\text{damping}} \\ = K_{\text{w}}w(x,y) + K_{\text{s}}\left(\frac{\partial^2 w(x,y)}{\partial x^2}+\frac{\partial^2 w(x,y)}{\partial y^2}\right) + C_{\text{d}}\frac{\partial w(x,y)}{\partial t} \end{gathered} \tag{27}$$

where K_{w}, K_{s} and C_{d} are spring, shear and damping parameters of the foundation. Inserting the Eqs. (25-27), into the Eq. (24), the equations of motion of the coated FG nanoplates can be calculated as follows:

$$\begin{gathered} (1-\lambda\nabla^2) \\ \begin{bmatrix} A_{11}\frac{\partial^2 u}{\partial x^2}+A_{66}\frac{\partial^2 u}{\partial y^2}+(A_{12}+A_{66})\frac{\partial^2 v}{\partial x\partial y} \\ -B_{11}\frac{\partial^3 w}{\partial x^3}-(B_{12}+2B_{66})\frac{\partial^3 w}{\partial x\partial y^2} \\ -C_{11}\frac{\partial^3 \psi}{\partial x^3}-(C_{11}+2C_{66})\frac{\partial^3 \psi}{\partial x\partial y^2} \end{bmatrix} \\ = (1-\mu\nabla^2)\left[I_0\ddot{u}_0 - I_1\frac{\partial\ddot{w}_0}{\partial x} - I_3\ddot{\psi}\right] \end{gathered} \tag{28}$$

$$\begin{gathered} (1-\lambda\nabla^2) \\ \begin{bmatrix} (A_{12}+A_{66})\frac{\partial^2 u}{\partial x\partial y}+A_{22}\frac{\partial^2 v}{\partial y^2}+A_{66}\frac{\partial^2 v}{\partial x^2} \\ -(B_{12}+2B_{66})\frac{\partial^3 w}{\partial x^2\partial y}-B_{22}\frac{\partial^3 w}{\partial y^3} \\ -(C_{12}+2C_{66})\frac{\partial^3 \psi}{\partial x^2\partial y}-C_{22}\frac{\partial^3 \psi}{\partial y^3} \end{bmatrix} \\ = (1-\mu\nabla^2)\left[I_0\ddot{v}_0 - I_1\frac{\partial\ddot{w}_0}{\partial y} - I_3\ddot{\psi}\right] \end{gathered} \tag{29}$$

$$\begin{gathered} (1-\lambda\nabla^2) \\ \begin{bmatrix} B_{11}\frac{\partial^3 u}{\partial x^3}+(B_{12}+2B_{66})\frac{\partial^3 u}{\partial x\partial y^2} \\ +(B_{12}+2B_{66})\frac{\partial^3 v}{\partial x^2\partial y}+B_{22}\frac{\partial^3 v}{\partial y^3}-D_{11}\frac{\partial^4 w}{\partial x^4} \\ -(2D_{12}+4D_{66})\frac{\partial^4 w}{\partial x^2\partial y^2}-D_{22}\frac{\partial^4 w}{\partial y^4} \\ -E_{11}\frac{\partial^4 \psi}{\partial x^4}-2(E_{12}+2E_{66})\frac{\partial^4 \psi}{\partial x^2\partial y^2}-E_{22}\frac{\partial^4 \psi}{\partial y^4} \end{bmatrix} \\ = (1-\mu\nabla^2)\begin{bmatrix} I_0\ddot{w}_0+I_1\left(\frac{\partial\ddot{u}_0}{\partial x}+\frac{\partial\ddot{v}_0}{\partial y}\right) \\ I_2\left(\frac{\partial^2\ddot{w}_0}{\partial x^2}+\frac{\partial^2\ddot{w}_0}{\partial y^2}\right)-I_4\left(\frac{\partial\ddot{\psi}}{\partial x}+\frac{\partial\ddot{\psi}}{\partial y}\right) \end{bmatrix} \end{gathered} \tag{30}$$

$$\begin{gathered} (1-\lambda\nabla^2) \\ \begin{bmatrix} C_{11}\frac{\partial^3 u}{\partial x^3}+(C_{12}+2C_{66})\frac{\partial^3 u}{\partial x\partial y^2}+(C_{12}+2C_{66})\frac{\partial^3 v}{\partial x^2\partial y} \\ +C_{22}\frac{\partial^3 v}{\partial y^3}-E_{11}\frac{\partial^4 w_0}{\partial x^4}-2(E_{12}+2E_{66})\frac{\partial^4 w_0}{\partial x^2\partial y^2} \\ -E_{22}\frac{\partial^4 w_0}{\partial x^4}-F_{11}\frac{\partial^4 \psi}{\partial x^4}-2(F_{12}+2F_{66})\frac{\partial^4 \psi}{\partial x^2\partial y^2} \\ -F_{22}\frac{\partial^4 \psi}{\partial y^4}+J_{44}\frac{\partial^2 \psi}{\partial y^2}+J_{55}\frac{\partial^2 \psi}{\partial x^2} \end{bmatrix} \\ = (1-\mu\nabla^2)\begin{bmatrix} I_3\left(\frac{\partial\ddot{u}_0}{\partial x}+\frac{\partial\ddot{v}_0}{\partial y}\right)-I_4\left(\frac{\partial^2\ddot{w}_0}{\partial x^2}+\frac{\partial^2\ddot{w}_0}{\partial y^2}\right) \\ -I_5\left(\frac{\partial^2\ddot{\psi}}{\partial x^2}+\frac{\partial^2\ddot{\psi}}{\partial y^2}\right) \end{bmatrix} \end{gathered} \tag{31}$$

The coefficients of the stiffnesses can be expressed as

$$\begin{gathered} \{A_{11},B_{11},C_{11},D_{11},E_{11},F_{11}\} \\ = \int Q_{11}\left\{1,z,f(z),z^2,zf(z),(f(z))^2\right\}\mathrm{d}x\mathrm{d}y\mathrm{d}z \\ \{A_{12},B_{12},C_{12},D_{12},E_{12},F_{12}\} \\ = \int Q_{12}\left\{1,z,f(z),z^2,zf(z),(f(z))^2\right\}\mathrm{d}x\mathrm{d}y\mathrm{d}z \\ \{A_{66},B_{66},C_{66},D_{66},E_{66},F_{66}\} \\ = \int Q_{66}\left\{1,z,f(z),z^2,zf(z),(f(z))^2\right\}\mathrm{d}x\mathrm{d}y\mathrm{d}z \end{gathered} \tag{32}$$

$$J_{44} = \int Q_{44}\left(f'(z)\right)^2 \mathrm{d}x\mathrm{d}y\mathrm{d}z\,, \qquad J_{44} = J_{55}$$

and

$$\{I_0, I_1, I_2, I_3, I_4, I_5\} = \int \rho(z)\left\{1, z, z^2, f(z), zf(z), \left(\Phi(z)\right)^2\right\}\mathrm{d}x\mathrm{d}y\mathrm{d}z \tag{33}$$

4. Analytical Solution

The Galerkin approach is used to consider the four unknown displacements and examine various boundary conditions. The expressions for the displacements using the Galerkin method can be written as follows:

$$\begin{aligned} u_0 &= \sum_{m=1}^{\infty}\sum_{n=1}^{\infty} U_{mn}.\frac{\partial X_m(x)}{\partial x}Y_n(y)e^{i\omega t} \\ v_0 &= \sum_{m=1}^{\infty}\sum_{n=1}^{\infty} V_{mn}.X_m(x)\frac{\partial Y_n(y)}{\partial y}e^{i\omega t} \\ \{w_0, \psi\} &= \sum_{m=1}^{\infty}\sum_{n=1}^{\infty}\{W_{mn}, \Psi_{mn},\}X_m(x)Y_n(y)\,e^{i\omega t} \end{aligned} \tag{34}$$

The parameters U_{mn}, V_{mn}, W_{mn} and Ψ_{mn} are defined as arbitrary. Here, *m* and *n* denote the mode numbers and ω is the natural frequency. Table 1 and Fig. 3 represent the functions $X_m(x)$ and $Y_n(y)$ that satisfy the simply supported and/or clamped boundary conditions.

By replacing the equation represented as "Eq. (34)" with the equations indicated as "Eqs. (28-31)", the result is obtained.

$$[K] + [C]\omega - [M]\omega^2 = 0 \tag{35}$$

where [K] and [M] are the rigidity matrix and mass matrix, respectively.

The elements K_{ij} and M_{ij} of the matrix [K] and [M] are given in Appendix A.

Here, $\alpha = m\pi/a$, $\beta = n\pi/b$.

5. Results and discussions

5.1 Validation study

Firstly, a comparative study is presented in Table 2 to validate the accuracy of our theoretical model and solution technique. The dimensionless frequencies of functionally graded graphene-reinforced composite (FG-GRC) simply supported plates are evaluated with various distribution patterns (Polymer, UD, FG-X, FG-O, and FG-V) and compared with results from previous studies. Specifically, our results are compared with those of Song *et al*. (2017), who used an exact First-Order Shear Deformation Theory (FSDT) model; Guo *et al*. (2018), who employed the Improved Moving Least Squares (IMLS) Ritz method and FSDT model; Jafari *et al*. (2021), who utilized the quasi-3D third-order shear deformation theory; and Chen *et al*. (2020), who applied the Rayleigh-Ritz method based on FSDT. The results for a square plate with dimensions

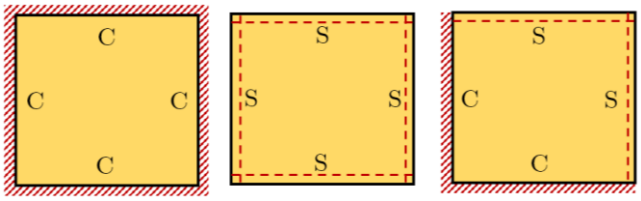

Fig. 3 Various boundary conditions of the FG GRC plate

Table 1 The admissible functions $X_m(x)$ and $Y_n(y)$ for different boundary conditions.

	Boundary conditions	
	At $x = 0, a$	At $y = 0, b$
SSSS	$X_m(0) = X_m''(0) = 0$ $X_m(a) = X_m''(a) = 0$	$Y_n(0) = Y_n''(0) = 0$ $Y_n(b) = Y_n''(b) = 0$
CCCC	$X_m(0) = X_m'(0) = 0$ $X_m(a) = X_m''(a) = 0$	$Y_n(0) = Y_n''(0) = 0$ $Y_n(b) = Y_n''(b) = 0$
CCSS	$X_m(0) = X_m'(0) = 0$ $X_m(a) = X_m''(a) = 0$	$Y_n(0) = Y_n'(0) = 0$ $Y_n(b) = Y_n''(b) = 0$
	The functions X_m and Y_n	
	$X_m(x)$	$Y_n(y)$
SSSS	$\sin(\alpha x)$	$\sin(\beta y)$
CCCC	$\sin^2(\alpha x)$	$\sin^2(\beta y)$
CCSS	$\sin(\alpha x)[\cos(\alpha x) - 1]$	$\sin(\beta y)[\cos(\beta y) - 1]$

a/h=10 and a graphene platelet weight fraction W_{GPL} of 1%, comprising a total of 10 layers, demonstrate that our findings are in close agreement with the existing data in the literature. This agreement confirms the correctness and accuracy of the developed formulation and solution method.

5.2 Parametric study

This section suggests the use of a composite plate composed of a mixture of epoxy and GPLs as the matrix and reinforcement materials, respectively. The mechanical properties of the epoxy and GPLs components are provided below:

Epoxy (matrix): $E_m = 3$ Gpa, $\nu_m = 0.34$, $\rho_m = 1200$ kg/m^3.

GPLs (reinforcement): $E_{GPL} = 1010$ Gpa, $\nu_{GPL} = 0.186$, $\rho_{GPL} = 1060$ kg/m^3.

The GNLs have a length $a_{GPL} = 2.5$ µm, thickness $h_{GPL} = 1.5$ nm and width $b_{GPL} = 1.5$ µm. The frequencies and foundation parameters are normalized using the following formulas:

$$\bar{\omega} = 10^2 h\sqrt{\frac{\rho_m}{E_m}}\omega \tag{36}$$

$$K_w = \frac{k_w a^2}{D}, \qquad K_s = \frac{k_s}{D}, \qquad C_d = c_d(hD\rho_c)^{-1} \tag{37}$$

where $D = \frac{E_c h^3}{12(1-\nu^2)}$.

5.2.1 Effect of the material distribution

To analyze the impact of various inhomogeneity exponents *p*, *k* and *e*, which are varied from 1 to 10, on the

Table 2 Comparison of dimensionless natural frequencies $(10^{-2}\bar{\omega})$ of FG-GRC plate $(SSSS, b = a = 10h, W_{GPL} = 1\%)$

Pattern	Ref.	(1,1)	(2,1)	(2,2)	(3,1)	(3,2)	(3,3)
Polymer	Song *et al*. (2017)	0.0584	0.1391	0.2132	0.2595	0.3251	-
	Chen *et al*. (2020)	0.0587	0.1406	0.2164	0.2641	0.3321	-
	Present	0.0584	0.1391	0.2132	0.2596	0.3253	0.4265
UD-GRC	Song	0.1216	0.2895	0.4436	0.5400	0.6767	0.8869
	Chen *et al*. (2020)	0.1220	0.2923	0.4499	0.5492	0.6907	-
	Guo *et al*. (2018)	0.1216	0.2895	0.4434	0.5400	0.6763	-
	Jafari and Kiani (2021)	0.1217	0.2903	0.4456	0.5430	0.6814	0.8950
	Present	0.1216	0.2895	0.4437	0.5402	0.6770	0.8877
X-GRC	Song *et al*. (2017)	0.1378	0.3249	0.4939	0.5984	0.7454	0.9690
	Chen *et al*. (2020)	0.1385	0.3289	0.5028	0.6112	0.7645	-
	Guo *et al*. (2018)	0.1378	0.3249	0.4937	0.5985	0.7452	-
	Jafari and Kiani (2021)	0.1392	0.3237	0.4868	0.5866	0.7254	0.9343
	Present	0.1366	0.3189	0.4809	0.5803	0.7191	0.9284
O-GRC	Song *et al*. (2017)	0.1020	0.2456	0.3796	0.4645	0.5860	0.7755
	Chen *et al*. (2020)	0.1023	0.2472	0.3835	0.4702	0.5949	-
	Guo *et al*. (2018)	0.1020	0.2455	0.3793	0.4645	0.5855	-
	Jafari and Kiani (2021)	0.0979	0.2376	0.3699	0.4545	0.5766	0.7690
	Present	0.1023	0.2470	0.3828	0.4691	0.5930	0.7870
V-GRC	Song *et al*. (2017)	0.1118	0.2673	0.4110	0.5013	0.6299	0.8287
	Guo *et al*. (2018)	0.1118	0.2673	0.4108	0.5013	0.6293	-
	Jafari and Kiani (2021)	0.1126	0.2696	0.4151	0.5068	0.6376	0.8405
	Present	0.1118	0.2674	0.4111	0.5015	0.6302	0.8294

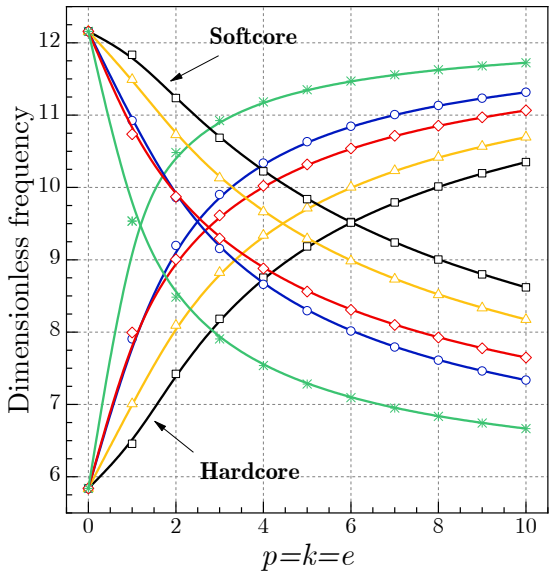

Fig. 4 Effect of the exponents p, k and e on the dimensionless frequencies of various types of coated plate $(SSSS, b = a = 10h, W_{GPL} = 1\%)$

dimensionless frequency $\bar{\omega}$ of coated FG GRC plate, Tables 3 and 4 in addition to Figs. 4 and 5 are performed. From both Table 3 and Fig. 4, The study considers two types of plates: hardcore and softcore. In the case of the hardcore plate, an increase in the values of p, k, and e results in a stiffer plate, leading to an increase in frequencies, regardless of the GPLs reinforcement patterns. On the other hand, for the softcore plate, an increase in p, k, and e has the opposite effect. When $p = k = e = 0$, the plate is fully composed of epoxy with no GPLs, while for the softcore plate, the highest proportion of GPLs is uniformly distributed.

On the other hand, Table 4 and Fig. 5 depicts the effect of weight fraction W_{GPL} (%) on the dimensionless critical buckling load of FG-GRC coated plates with different GPL reinforcement patterns. It is evident that an increase in the weight fraction results in improved plate stiffness, leading to an increase in dimensionless frequencies, particularly in the case of the softcore plate.

5.2.2 Effect of the plate geometry

Table 5 presents the dimensionless frequency $\bar{\omega}$ of coated FG GRC plate versus the aspect ratio *b/a*. The fully simply supported plate has the lowest stiffness, while the stiffer plate is the fully clamped one. The influence of the aspect ratio on the dimensionless frequencies of various types of coated hardcore FG-A GRC plates is plotted in Fig. 6. It is clear that the vibrational frequencies rise with the decrease of both the thickness ratio and the aspect ratio.

5.2.3 Effect of nonlocal and length-scale parameters

The action of the plate size-dependent determined by the

Table 4 Effect of the weigh fraction and the shell structure on the dimensionless frequency of FG GRC plate $(SSSS, p = k = e = 2)$

p	k	e	Hardcore					Softcore				
			FG-A	FG-B	FG-C	FG-D	FG-E	FG-A	FG-B	FG-C	FG-D	FG-E
2	2	2	6.1554	6.2149	6.1775	6.2104	6.2662	6.2993	6.2406	6.2775	6.2447	6.1891
		5	6.1665	6.2406	6.1775	6.2104	6.2662	6.2884	6.2149	6.2775	6.2447	6.1891
		10	6.1715	6.2523	6.1775	6.2104	6.2662	6.2834	6.2032	6.2775	6.2447	6.1891
	5	2	6.1665	6.2406	6.1940	6.2104	6.3045	6.2884	6.2149	6.2611	6.2447	6.1501
		5	6.1802	6.2726	6.1940	6.2104	6.3045	6.2748	6.1826	6.2611	6.2447	6.1501
		10	6.1865	6.2871	6.1940	6.2104	6.3045	6.2686	6.1679	6.2611	6.2447	6.1501
	10	2	6.1715	6.2523	6.2015	6.2104	6.3218	6.2834	6.2032	6.2537	6.2447	6.1324
		5	6.1865	6.2871	6.2015	6.2104	6.3218	6.2686	6.1679	6.2537	6.2447	6.1324
		10	6.1933	6.3029	6.2015	6.2104	6.3218	6.2618	6.1518	6.2537	6.2447	6.1324
5	2	2	6.1780	6.2149	6.2113	6.2609	6.2662	6.2771	6.2406	6.2441	6.1943	6.1891
		5	6.1947	6.2406	6.2113	6.2609	6.2662	6.2606	6.2149	6.2441	6.1943	6.1891
		10	6.2022	6.2523	6.2113	6.2609	6.2662	6.2531	6.2032	6.2441	6.1943	6.1891
	5	2	6.1947	6.2406	6.2361	6.2609	6.3045	6.2606	6.2149	6.2193	6.1943	6.1501
		5	6.2154	6.2726	6.2361	6.2609	6.3045	6.2400	6.1826	6.2193	6.1943	6.1501
		10	6.2248	6.2871	6.2361	6.2609	6.3045	6.2306	6.1679	6.2193	6.1943	6.1501
	10	2	6.2022	6.2523	6.2474	6.2609	6.3218	6.2531	6.2032	6.2080	6.1943	6.1324
		5	6.2248	6.2871	6.2474	6.2609	6.3218	6.2306	6.1679	6.2080	6.1943	6.1324
		10	6.2351	6.3029	6.2474	6.2609	6.3218	6.2203	6.1518	6.2080	6.1943	6.1324
10	2	2	6.1922	6.2149	6.2325	6.2924	6.2662	6.2631	6.2406	6.2230	6.1624	6.1891
		5	6.2124	6.2406	6.2325	6.2924	6.2662	6.2431	6.2149	6.2230	6.1624	6.1891
		10	6.2216	6.2523	6.2325	6.2924	6.2662	6.2339	6.2032	6.2230	6.1624	6.1891
	5	2	6.2124	6.2406	6.2625	6.2924	6.3045	6.2431	6.2149	6.1928	6.1624	6.1501
		5	6.2375	6.2726	6.2625	6.2924	6.3045	6.2180	6.1826	6.1928	6.1624	6.1501
		10	6.2489	6.2871	6.2625	6.2924	6.3045	6.2065	6.1679	6.1928	6.1624	6.1501
	10	2	6.2216	6.2523	6.2761	6.2924	6.3218	6.2339	6.2032	6.1790	6.1624	6.1324
		5	6.2489	6.2871	6.2761	6.2924	6.3218	6.2065	6.1679	6.1790	6.1624	6.1324
		10	6.2613	6.3029	6.2761	6.2924	6.3218	6.1940	6.1518	6.1790	6.1624	6.1324

Table 5 Dimensionless frequency of coated FG GRC plate versus the aspect ratio $(a = 10h, \mu = \lambda = C_t = K_w = K_s = 0)$

BCs.	b/a	Hardcore					Softcore				
		FG-A	FG-B	FG-C	FG-D	FG-E	FG-A	FG-B	FG-C	FG-D	FG-E
SSSS	0,5	17.8321	31.5498	24.4626	36.4387	21.7006	38.5835	27.8779	47.5306	23.4835	40.9539
	1	7.4219	13.1074	13.4453	14.7592	9.0056	15.9388	15.3224	20.0924	9.8609	17.3008
	2	4.6883	8.6591	11.0663	10.1845	5.6839	10.5155	12.6113	13.9692	6.2448	11.4752
	3	4.1758	7.9329	10.6697	9.5831	5.0617	9.6321	12.1593	13.1451	5.5648	10.5184
CCCC	0,5	17.8321	31.5498	24.4626	36.4387	21.7006	38.5835	27.8779	47.5306	23.4835	40.9539
	1	7.4219	13.1074	13.4453	14.7592	9.0056	15.9388	15.3224	20.0924	9.8609	17.3008
	2	4.6883	8.6591	11.0663	10.1845	5.6839	10.5155	12.6113	13.9692	6.2448	11.4752
	3	4.1758	7.9329	10.6697	9.5831	5.0617	9.6321	12.1593	13.1451	5.5648	10.5184
CCSS	0,5	19.9688	39.8152	19.4751	34.5463	24.3232	45.3741	26.5869	45.9066	26.2256	44.5276
	1	10.9142	16.5712	8.0932	14.3093	13.2693	18.8847	11.2350	19.6190	14.4143	19.0676
	2	8.9836	11.4887	5.1101	9.4464	10.9223	13.0927	7.1282	13.0502	11.8638	13.2888
	3	8.6640	10.8107	4.5510	8.6535	10.5346	12.3200	6.3543	11.9665	11.4387	12.5052

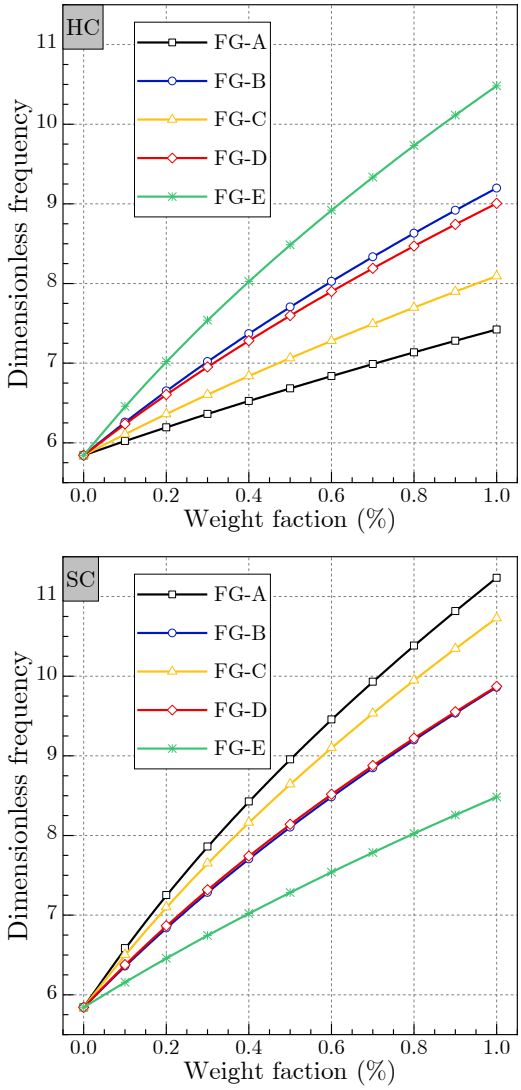

Fig. 5 Effect of weight fraction W_{GPL} on the dimensionless frequencies of coated plate $(SSSS, p = k = e = 2, b = a = 10h, C_d = K_w = K_s = 0, W_{GPL} = 1\%)$

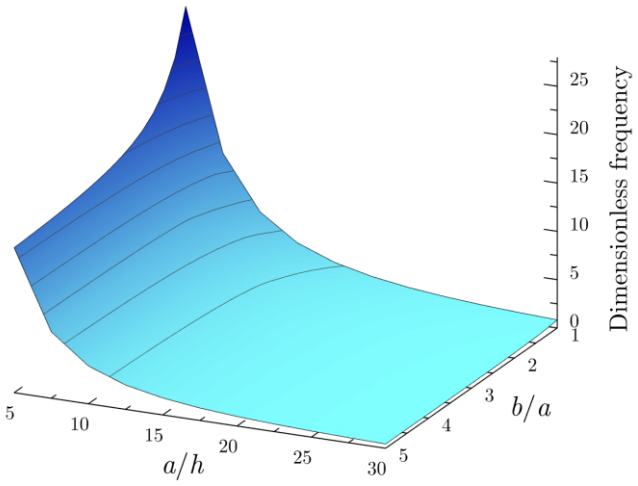

Fig. 6 Effect of the aspect ratio on the dimensionless frequencies of various types of coated hardcore FG-A GRC plate $(SSSS, p = k = e = 2, a = 10h, C_d = K_w = K_s = 0, W_{GPL} = 1\%)$

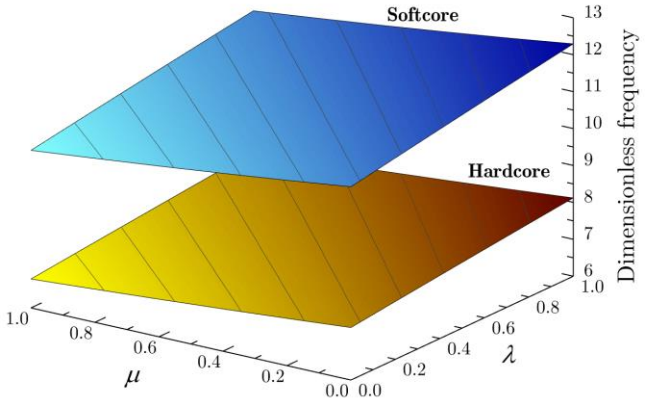

Fig. 7 Effect of nonlocal and length-scale parameters on the dimensionless frequencies of FG-A GRC plate $(SSSS, p = k = e = 2, b = a = 10h, C_d = K_w = K_s = 0, W_{GPL} = 1\%)$

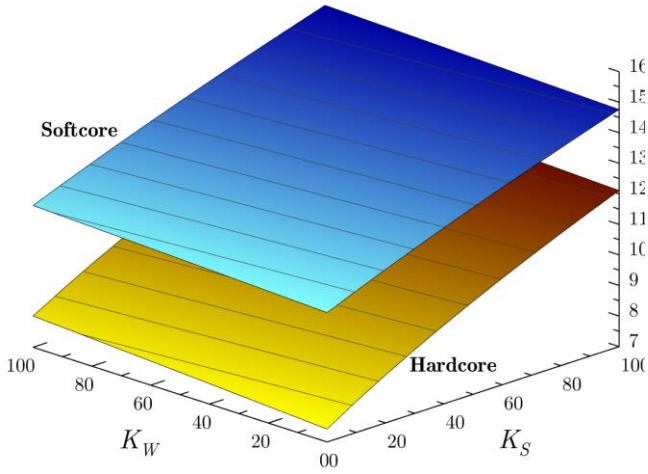

Fig. 8 Effect of the elastic foundation parameters on the dimensionless frequencies of FG-A GRC plate $(SSSS, p = k = e = 2, b = a = 10h, C_d = 0, W_{GPL} = 1\%)$

nonlocal and length-scale parameters on the dimensionless frequency of FG-A GRC plate is examined in Table 6. Fig. 7 demonstrate the impact of nonlocal parameter μ and length-scale parameter λ on the dimensionless frequency of the FG GRC coated plate under different boundary conditions to showcase the size-dependent effect. The μ and λ parameters are varied from 0 to 1. It is evident from this figure that, regardless of boundary conditions, the inclusion of the nonlocal parameter leads to a decrease in plate stiffness and a subsequent reduction in dimensionless frequencies, unlike the length-scale parameter. Moreover, the dimensionless frequency is observed to decrease with an increase in the length-scale parameter.

5.2.4 Effect of viscoelastic Winkler/Pasternak foundation

To investigate the vibrational behavior of coated FG plates supported by a Winkler/Pasternak viscoelastic foundation, a parametric study is conducted by varying various foundation parameters such as the Winkler foundation parameter K_W, the Pasternak foundation parameters K_S, and the damping coefficient C_d. Table 7

Table 6 Dimensionless frequency $\bar{\omega}$ of coated FG GRC nanoplate versus nonlocal and length-scale parameters $(SSSS, p = 2,\ b = a = 10h, C_t = K_w = K_s = 0)$

μ	λ	Hardcore					Softcore				
		FG-A	FG-B	FG-C	FG-D	FG-E	FG-A	FG-B	FG-C	FG-D	FG-E
0	0	7.4219	9.1980	8.0932	9.0056	10.4822	11.2350	9.8609	10.7302	9.8720	8.4837
	0,25	7.6029	9.4222	8.2904	9.2251	10.7377	11.5089	10.1013	10.9917	10.1126	8.6905
	0,5	7.7796	9.6412	8.4831	9.4395	10.9873	11.7764	10.3361	11.2472	10.3477	8.8925
	0,75	7.9524	9.8554	8.6716	9.6492	11.2313	12.0380	10.5657	11.4970	10.5775	9.0900
	1	8.1215	10.0650	8.8560	9.8544	11.4702	12.2940	10.7904	11.7415	10.8024	9.2833
0,25	0	7.2453	8.9791	7.9006	8.7913	10.2328	10.9677	9.6263	10.4748	9.6370	8.2818
	0,25	7.4219	9.1980	8.0932	9.0056	10.4822	11.2350	9.8609	10.7302	9.8720	8.4837
	0,5	7.5945	9.4118	8.2813	9.2149	10.7258	11.4962	10.0901	10.9796	10.1014	8.6809
	0,75	7.7631	9.6209	8.4652	9.4196	10.9641	11.7515	10.3142	11.2234	10.3258	8.8737
	1	7.9282	9.8254	8.6452	9.6199	11.1972	12.0014	10.5336	11.4621	10.5454	9.0624
0,5	0	7.0807	8.7752	7.7211	8.5916	10.0003	10.7185	9.4076	10.2369	9.4181	8.0937
	0,25	7.2533	8.9891	7.9093	8.8010	10.2441	10.9798	9.6369	10.4864	9.6477	8.2910
	0,5	7.4219	9.1980	8.0932	9.0056	10.4822	11.2350	9.8609	10.7302	9.8720	8.4837
	0,75	7.5868	9.4023	8.2729	9.2056	10.7150	11.4846	10.0800	10.9685	10.0912	8.6721
	1	7.7481	9.6023	8.4489	9.4014	10.9429	11.7288	10.2943	11.2018	10.3058	8.8565
0,75	0	6.9269	8.5845	7.5533	8.4049	9.7830	10.4856	9.2032	10.0145	9.2135	7.9178
	0,25	7.0957	8.7938	7.7375	8.6098	10.0215	10.7413	9.4275	10.2586	9.4381	8.1108
	0,5	7.2607	8.9982	7.9173	8.8099	10.2544	10.9909	9.6467	10.4970	9.6575	8.2993
	0,75	7.4219	9.1980	8.0932	9.0056	10.4822	11.2350	9.8609	10.7302	9.8720	8.4837
	1	7.5798	9.3936	8.2653	9.1971	10.7051	11.4740	10.0706	10.9584	10.0819	8.6641
1	0	6.7826	8.4057	7.3961	8.2299	9.5793	10.2673	9.0116	9.8059	9.0216	7.7529
	0,25	6.9480	8.6106	7.5763	8.4305	9.8128	10.5176	9.2312	10.0450	9.2416	7.9419
	0,5	7.1095	8.8108	7.7524	8.6264	10.0409	10.7620	9.4458	10.2784	9.4564	8.1265
	0,75	7.2674	9.0065	7.9246	8.8180	10.2639	11.0011	9.6556	10.5067	9.6664	8.3070
	1	7.4219	9.1980	8.0932	9.0056	10.4822	11.2350	9.8609	10.7302	9.8720	8.4837

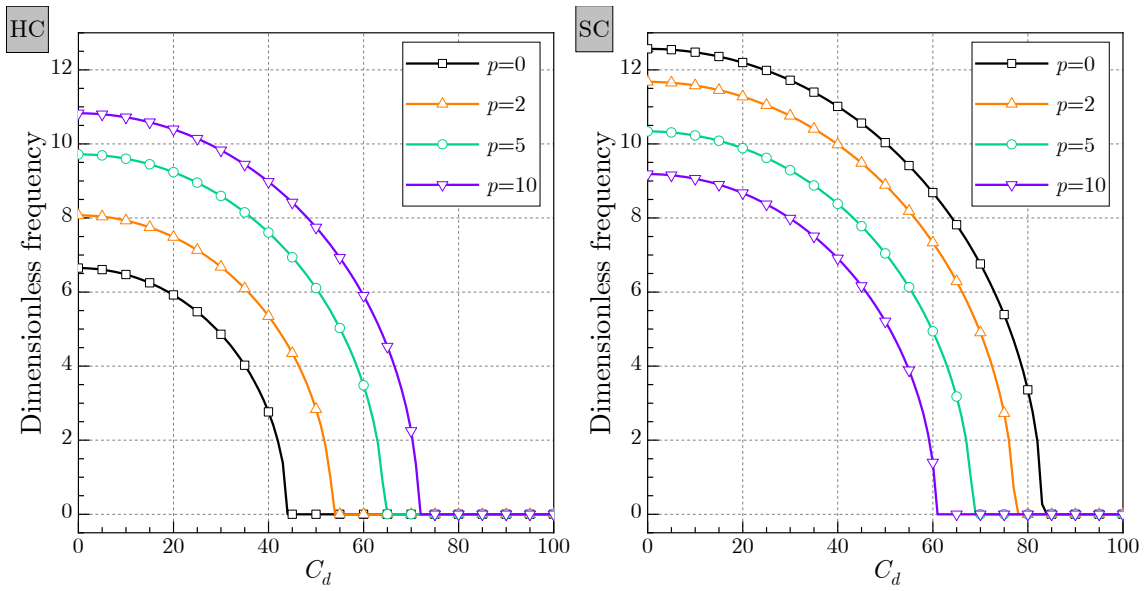

Fig. 9 Effect of the damping coefficient on the dimensionless frequencies of FG-A GRC plate for different length-scale and nonlocal parameters $(SSSS, b = a = 10h,\ K_w = K_s = 10, W_{GPL} = 1\%)$

Table 7 Dimensionless frequency $\bar{\omega}$ of coated FG GRC plate versus elastic foundation parameters ($SSSS, p = 2, b = a = 10h, \mu = \lambda = 0$)

C_d	K_W	K_S	Hardcore					Softcore				
			FG-A	FG-B	FG-C	FG-D	FG-E	FG-A	FG-B	FG-C	FG-D	FG-E
0	10	10	8.0725	9.7309	8.6937	9.5490	10.9529	11.6756	10.3598	11.1906	10.3709	9.0585
		50	10.0883	11.4596	10.5921	11.3051	12.5144	13.1521	11.9985	12.7237	12.0098	10.8943
		100	12.1464	13.3084	12.5682	13.1750	14.2272	14.7918	13.7754	14.4124	13.7872	12.8245
	50	10	8.2990	9.9197	8.9045	9.7413	11.1211	11.8336	10.5375	11.3554	10.5485	9.2611
		50	10.2705	11.6204	10.7658	11.4680	12.6618	13.2925	12.1522	12.8688	12.1636	11.0633
		100	12.2981	13.4471	12.7149	13.3151	14.3571	14.9169	13.9095	14.5407	13.9213	12.9684
	100	10	8.5738	10.1509	9.1612	9.9766	11.3278	12.0281	10.7554	11.5580	10.7665	9.5083
		50	10.4938	11.8184	10.9791	11.6685	12.8438	13.4660	12.3417	13.0480	12.3531	11.2710
		100	12.4852	13.6185	12.8960	13.4881	14.5178	15.0717	14.0753	14.6995	14.0871	13.1461
10	2	2	7.9297	9.6126	8.5613	9.4285	10.8479	11.5771	10.2488	11.0878	10.2597	8.9314
		5	9.9744	11.3594	10.4837	11.2035	12.4226	13.0647	11.9028	12.6333	11.9140	10.7888
		10	12.0520	13.2222	12.4770	13.0880	14.1466	14.7142	13.6921	14.3327	13.7037	12.7351
	5	2	8.1602	9.8038	8.7752	9.6233	11.0177	11.7364	10.4283	11.2541	10.4393	9.1368
		5	10.1587	11.5216	10.6592	11.3679	12.5711	13.2061	12.0577	12.7795	12.0689	10.9594
		10	12.2049	13.3618	12.6247	13.2290	14.2772	14.8399	13.8270	14.4617	13.8387	12.8800
	10	2	8.4396	10.0376	9.0356	9.8613	11.2263	11.9325	10.6485	11.4585	10.6595	9.3873
		5	10.3844	11.7212	10.8745	11.5701	12.7544	13.3807	12.2486	12.9599	12.2599	11.1691
		10	12.3934	13.5343	12.8071	13.4031	14.4388	14.9955	13.9938	14.6214	14.0055	13.0588
20	2	2	7.4851	9.2488	8.1511	9.0575	10.5266	11.2764	9.9082	10.7734	9.9187	8.5387
		5	9.6248	11.0532	10.1515	10.8931	12.1431	12.7990	11.6109	12.3583	11.6217	10.4660
		10	11.7642	12.9601	12.1992	12.8233	13.9018	14.4788	13.4391	14.0909	13.4504	12.4629
	5	2	7.7289	9.4473	8.3755	9.2601	10.7015	11.4399	10.0938	10.9445	10.1044	8.7534
		5	9.8156	11.2198	10.3326	11.0621	12.2950	12.9433	11.7696	12.5077	11.7805	10.6419
		10	11.9208	13.1025	12.3503	12.9672	14.0347	14.6065	13.5765	14.2221	13.5879	12.6109
	10	2	8.0233	9.6897	8.6479	9.5072	10.9162	11.6410	10.3211	11.1546	10.3317	9.0144
		5	10.0490	11.4247	10.5546	11.2698	12.4823	13.1214	11.9651	12.6920	11.9760	10.8576
		10	12.1138	13.2784	12.5366	13.1448	14.1991	14.7646	13.7464	14.3844	13.7577	12.7935

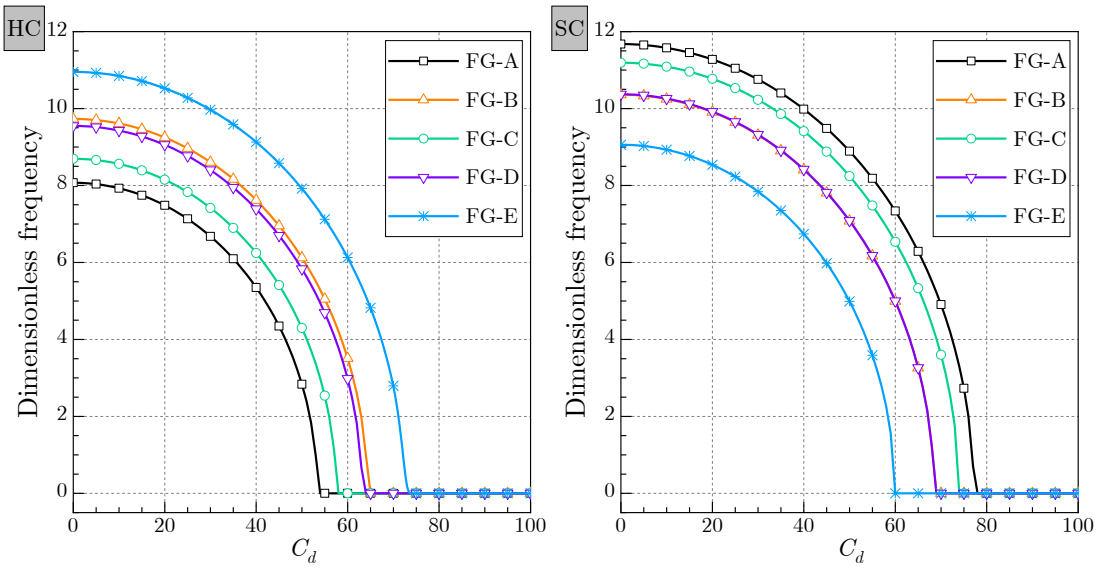

Fig. 10 Effect of the damping coefficient on the dimensionless frequencies of FG-A GRC plate for different length-scale and nonlocal parameters ($SSSS, p = k = e = 2, b = a = 10h, K_w = K_s = 10, W_{GPL} = 1\%$)

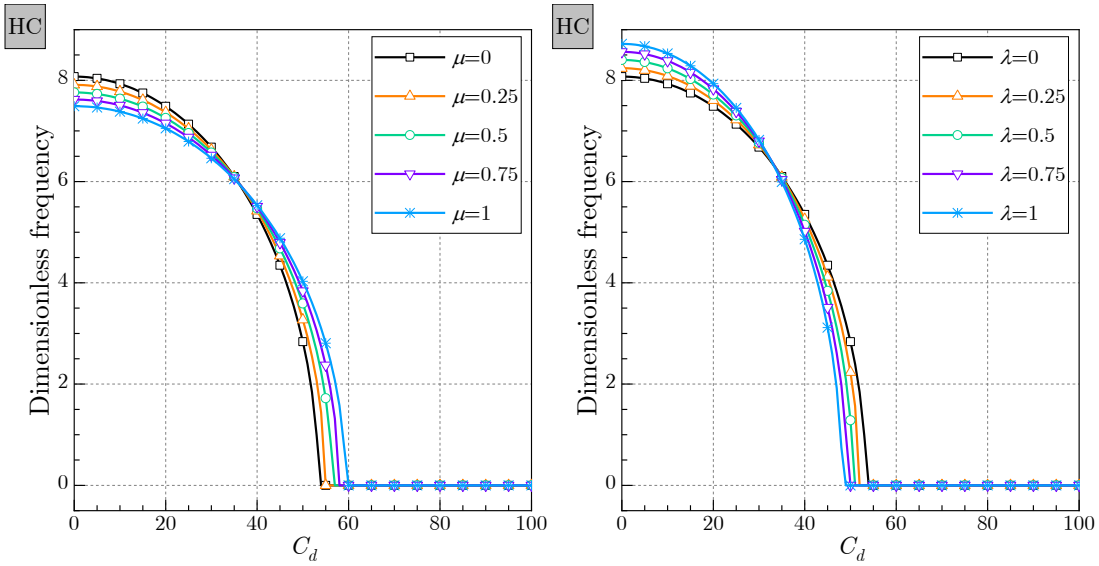

Fig. 11 Effect of the damping coefficient on the dimensionless frequencies of hardcore FG-A GRC nanoplate for different length-scale and nonlocal parameters $(CSCS, p = k = e = 2, b = a = 10h, K_w = K_s = 10, W_{GPL} = 1\%)$

shows the impact of these parameters on dimensional frequencies. To better understand the effect of the foundation medium, Figs. 8-11 are plotted. Fig. 8 displays the dimensionless frequencies of hardcore/softcore FG-A coated plates influenced by Winkler/Pasternak elastic foundation. The inclusion of the foundation improves the rigidity of the plates, where an increase in the parameters K_W and K_S results in an increase in the values of the dimensionless frequency. Furthermore, the hardcore FG plate is more affected by the foundation parameters than the softcore FG plate.

Fig. 9 depicts the relationship between the dimensionless frequency and damping coefficient of the viscoelastic medium for various inhomogeneity parameter *p*, *k*, and *e* of SSSS hardcore/softcore FG-A GRC plate. The figure shows that increasing the damping coefficient leads to a continuous decrease in the dimensionless frequency, ultimately resulting in a decrease in the natural frequency. Similar to previous illustrations, and unlike the softcore plates, the increase in the exponents *p*, *k*, and *e* leads to an increment in the frequencies of the hardcore FG-A GRC plates.

As same as Fig. 9, the damping coefficient effect of the viscoelastic medium for various FG GRC patterns is investigated in Fig. 10. The frequency of CSCS FG GRC nanoplate will be damped gradually as the damping coefficient of the viscoelastic foundation is increased.

At the end, the influence of the size-dependence is shown in Fig. 11. Once again it can be shown that the nonlocal parameters decrease the plate rigidity, unlike the length-scale parameter.

6. Conclusions

This research paper examines the vibrational behavior of a newly coated composite plate that is strengthened with functionally graded graphene. The aim is to investigate how these structures respond to vibration by using a formulated equation of motion that is solved analytically through the Galerkin method. To estimate the effective Young's modulus of the GRC coated plate, the Halpin-Tsai model is utilized, while the Poisson's ratio and mass density are calculated using the rule of mixture. The study analyzes two types of FG GRC coated plates, namely hardcore and softcore, and considers five different patterns of GPL distribution. The research conducts a thorough analysis of the effects of material and geometric properties, and the parametric studies demonstrate that:

• The study finds that the hardcore FG-A GRC plate has a better response compared to other plate patterns due to its higher stiffness.

• Increasing the weight fraction leads to an improvement in the stiffness of FG-GRC plates.

• Augmenting the length-to-width and length-to-thickness ratios results in an overall decrease in the stiffness of the GRC plate, leading to lower natural frequencies.

• The dimensionless frequencies of the FG GRC coated plate decrease as the nonlocal parameter increases, indicating a reduction in the plate stiffness. On the other hand, the length-scale parameter has an inverse effect, where increasing it leads to a decrease in dimensionless frequencies.

• An increase in the values of the dimensionless frequency is observed as the viscoelastic Winkler/Pasternak factors are increased.

Acknowledgement

The authors gratefully acknowledge the funding of the Deanship Graduate Studies and Scientic Research, Jazan University, Saudi Arabia, through project number RG24-M029.

References

Abo-bakr, R.M., Abo-bakr, H.M., Mohamed, S.A. and Eltaher, M.A. (2020), "Optimal weight for buckling of FG beam under variable axial load using pareto optimality", *Compos. Struct.*, **258**, 113193. https://doi.org/10.1016/j.compstruct.2020.113193

Anirudh, B., Ganapathi, M., Anant, C. and Polit, O. (2019), "A comprehensive analysis of porous graphene-reinforced curved beams by finite element approach using higher-order structural theory: Bending, vibration and buckling", *Compos. Struct.*, **222**, 110899. https://doi.org/10.1016/j.compstruct.2019.110899

Chen, D., Yang, J. and Kitipornchai, S. (2017), "Nonlinear vibration and postbuckling of functionally graded graphene reinforced porous nanocomposite beams", *Compos. Sci. Technol.*, **142**, 235-245. http://doi.org/10.1016/j.compscitech.2017.02.008

Chen, J., Cui, P. and Li, Q.S. (2020), "Free vibrations of functionally graded graphene-reinforced composite blades with varying cross-sections", *Int. J. Struct. Stabil. Dyn.*, **20**(14), 2043006. https://doi.org/10.1142/S0219455420430063

Daikh, A.A. and Zenkour, A.M. (2020), "Bending of functionally graded sandwich nanoplates resting on Pasternak foundation under different boundary conditions", *J. Appl. Comput. Mech.*, **6**, 1245-1259. https://doi.org/10.22055/JACM.2020.33136.2166

Daikh, A.A. and Megueni, A. (2018), "Thermal buckling analysis of functionally graded sandwich plates", *J. Therm. Stress.*, **41**(2), 139-159. https://doi.org/10.1080/01495739.2017.139364

Daikh, A.A., Drai, A., Bensaid, I., Houari, M.S.A. and Tounsi, A. (2020b), "On vibration of functionally graded sandwich nanoplates in the thermal environment", *J. Sand. Struct. Mater.*, 1099636220909790. https://doi.org/10.1177/1099636220909790

Daikh, A.A., Houari, M.S.A. and Tounsi, A. (2019), "Buckling analysis of porous FGM sandwich nanoplates due to heat conduction via nonlocal strain gradient theory", *Eng. Res. Exp.*, **1**(1), 015022. https://orcid.org/0000-0002-4666-2750

Daikh, A.A., Drai, A., Houari M.S.A, and Eltaher, M.A. (2020a), "Static analysis of multilayer nonlocal strain gradient nanobeam reinforced by carbon nanotubes", *Steel Compos. Struct.*, **36**(6), 643-656. https://doi.org/10.12989/scs.2020.36.6.64

Dastjerdi, S., Malikan, M., Dimitri, R. and Tornabene, F. (2021), "Nonlocal elasticity analysis of moderately thick porous functionally graded plates in a hygro-thermal environment", *Compos. Struct.*, 112925. https://doi.org/10.1016/j.compstruct.2020.112925

Dong, Y. H., He, L. W., Wang, L., Li, Y. H. and Yang, J. (2018), "Buckling of spinning functionally graded graphene reinforced porous nanocomposite cylindrical plates: an analytical study", *Aerosp. Sci. Technol.*, **82**, 466-478. https://doi.org/10.1016/j.ast.2018.09.037

Ebrahimi, F. and Barati, M.R. (2018), "Damping vibration analysis of graphene sheets on viscoelastic medium incorporating hygro-thermal effects employing nonlocal strain gradient theory", *Compos. Struct.*, **185**, 241-253. https://doi.org/10.1016/j.compstruct.2017.10.021

Ebrahimi, F. and Dabbagh, A. (2020), "Viscoelastic wave propagation analysis of axially motivated double-layered graphene sheets via nonlocal strain gradient theory", *Wave. Random Complex Med.*, **30**(1), 157-176. https://doi.org/10.1080/17455030.2018.1490505

Eltaher, M.A. and Mohamed, N. (2020), "Nonlinear stability and vibration of imperfect CNTs by Doublet mechanics", *Appl. Math. Comput.*, **382**, 125311. https://doi.org/10.1016/j.amc.2020.125311

Eltaher, M.A., Attia, M.A. and Wagih, A. (2020b), "Predictive model for indentation of elasto-plastic functionally graded composites", *Compos. Part B Eng.*, 108129. https://doi.org/10.1016/j.compositesb.2020.108129

Eltaher, M.A., Mohamed, N. and Mohamed, S.A. (2020a), "Nonlinear buckling and free vibration of curved CNTs by doublet mechanics", *Smart Struct. Syst.*, **26**(2), 213-226. https://doi.org/10.12989/sss.2020.26.2.213

Emam, S.A., Eltaher, M.A., Khater, M.E. and Abdalla, W.S. (2018), "Postbuckling and free vibration of multilayer imperfect nanobeams under a pre-stress load", *Appl. Sci.*, **8**(11), 2238. https://doi.org/10.3390/app8112238

Eringen, A.C. (1983), "On differential equations of nonlocal elasticity and solutions of screw dislocation and surface waves", *J. Appl. Phys.*, **54**(9), 4703-4710. https://doi.org/10.1063/1.332803

Fattahi, A.M., Sahmani, S. and Ahmed, N.A. (2019), "Nonlocal strain gradient beam model for nonlinear secondary resonance analysis of functionally graded porous micro/nano-beams under periodic hard excitations", *Mech. Based Des. Struct.*, 1-30. https://doi.org/10.1080/15397734.2019.1624176

Garcia-Macias, E., Rodriguez-Tembleque, L. and Saez, A. (2018), "Bending and free vibration analysis of functionally graded graphene vs. carbon nanotube reinforced composite plates", *Compos. Struct.*, **186**, 123-138. https://doi.org/10.1016/j.compstruct.2017.11.076

Guo, H., Cao, S., Yang, T. and Chen, Y. (2018), "Vibration of laminated composite quadrilateral plates reinforced with graphene nanoplatelets using the element-free IMLS-Ritz method", *Int. J. Mech. Sci.*, **142**, 610-621. https://doi.org/10.1016/j.ijmecsci.2018.05.029

Hamed M.A., R.M. Abu-bakr, Mohamed, S.A. and Eltaher, M.A., (2020b), "Influence of axial load function and optimization on static stability of sandwich functionally graded beams with porous core", *Eng. Comput.*, **36**(4), 1929-1946. https://doi.org/10.1007/s00366-020-01023-w

Hamed, M.A., Mohamed, S.A. and Eltaher, M.A. (2020a), "Buckling analysis of sandwich beam rested on elastic foundation and subjected to varying axial in-plane loads", *Steel Compos. Struct.*, **34**(1), 75-89. https://doi.org/10.12989/scs.2020.34.1.075

Huang, Y., Yang, Z., Liu, A. and Fu, J. (2018), "Nonlinear buckling analysis of functionally graded graphene reinforced composite shallow arches with elastic rotational constraints under uniform radial load", *Materials*, **11**(6), 910. https://doi.org/10.3390/ma11060910

Jafari, P. and Kiani, Y. (2021), "Free vibration of functionally graded graphene platelet reinforced plates: A quasi 3D shear and normal deformable plate model", *Compos. Struct.*, **275**, 114409. https://doi.org/10.1016/j.compstruct.2021.114409

Jalaei, M.H. and Civalek, Ö. (2019), "A nonlocal strain gradient refined plate theory for dynamic instability of embedded graphene sheet including thermal effects", *Compos. Struct.*, **220**, 209-220. https://doi.org/10.1016/j.compstruct.2019.03.086

Karami, B. and Shahsavari, D. (2020), "On the forced resonant vibration analysis of functionally graded polymer composite doubly-curved nanoplates reinforced with graphene-nanoplatelets", *Comput. Meth. Appl. Mech. Eng.*, **359**, 112767. https://doi.org/10.1016/j.cma.2019.112767

Liu, D., Kitipornchai, S., Chen, W. and Yang, J. (2018), "Three-dimensional buckling and free vibration analyses of initially stressed functionally graded graphene reinforced composite cylindrical plate", *Compos. Struct.*, **189**, 560-569. https://doi.org/10.1016/j.compstruct.2018.01.106

Liu, D., Li, Z., Kitipornchai, S. and Yang, J. (2019), « Three-dimensional free vibration and bending analyses of functionally graded graphene nanoplatelets-reinforced nanocomposite annular plates", *Compos. Struct.*, **229**, 111453. https://doi.org/10.1016/j.compstruct.2019.111453

Mao, J.J. and Zhang, W. (2019), "Buckling and post-buckling

analyses of functionally graded graphene reinforced piezo-electric plate subjected to electric potential and axial forces", *Compos. Struct.*, **216**, 392-405. https://doi.org/10.1016/j.compstruct.2019.02.095

Mohamed, N., Mohamed, S.A. and Eltaher, M.A. (2020), "Buckling and post-buckling behaviors of higher order carbon nanotubes using energy-equivalent model", *Eng. Comput.*, 1-14. https://doi.org/10.1007/s00366-020-00976-2

Polit, O., Anant, C., Anirudh, B. and Ganapathi, M. (2019), "Functionally graded graphene reinforced porous nanocomposite curved beams: Bending and elastic stability using a higher-order model with thickness stretch effect", *Compos. Part B Eng.*, **166**, 310-327. https://doi.org/10.1016/j.compositesb.2018.11.074

Rahimi, A., Alibeigloo, A. and Safarpour, M. (2020), "Three-dimensional static and free vibration analysis of graphene platelet–reinforced porous composite cylindrical plate", *J. Vib. Control*, 1077546320902340. https://doi.org/10.1177/1077546320902340

Reddy, J.N. (1990), "A general non-linear third-order theory of plates with moderate thickness", *Int. J. Non-Linear Mech.*, **25**(6), 677-686. https://doi.org/10.1016/0020-7462(90)90006-U

Sahmani, S., Aghdam, M. M. and Rabczuk, T. (2018), "Nonlinear bending of functionally graded porous micro/nano-beams reinforced with graphene platelets based upon nonlocal strain gradient theory", *Compos. Struct.*, **186**, 68-78. https://doi.org/10.1016/j.compstruct.2017.11.082

Shahgholian, D., Safarpour, M., Rahimi, A.R. and Alibeigloo, A. (2020), "Buckling analyses of functionally graded graphene-reinforced porous cylindrical plate using the Rayleigh–Ritz method", *Acta Mechanica*, 1-16. https://doi.org/10.1007/s00707-020-02616-8

Shen, H.S., Xiang, Y. and Lin, F. (2017a), "Thermal buckling and postbuckling of functionally graded graphene-reinforced composite laminated plates resting on elastic foundations", *Thin Wall. Struct.*, **118**, 229-237. http://doi.org/10.1016/j.tws.2017.05.006

Shen, H.S., Xiang, Y. and Lin, F. (2017b), "Nonlinear bending of functionally graded graphene-reinforced composite laminated plates resting on elastic foundations in thermal environments", *Compos. Struct.*, **170**, 80-90. http://doi.org/10.1016/j.compstruct.2017.03.001

Song, M., Kitipornchai, S. and Yang, J. (2017), "Free and forced vibrations of functionally graded polymer composite plates reinforced with graphene nanoplatelets", *Compos. Struct.*, **159**, 579-588. https://doi.org/10.1016/j.compstruct.2016.09.070

Song, M., Yang, J. and Kitipornchai, S. (2018), "Bending and buckling analyses of functionally graded polymer composite plates reinforced with graphene nanoplatelets", *Compos. Part B Eng.*, **134**, 106-113. https://doi.org/10.1016/j.compositesb.2017.09.043

Tam, M., Yang, Z., Zhao, S. and Yang, J. (2019), « Vibration and buckling characteristics of functionally graded graphene nanoplatelets reinforced composite beams with open edge cracks", *Materials*, **12**(9), 1412. https://doi.org/10.3390/ma12091412

Tam, M., Yang, Z., Zhao, S., Zhang, H., Zhang, Y. and Yang, J. (2020), "Nonlinear bending of elastically restrained functionally graded graphene nanoplatelet reinforced beams with an open edge crack", *Thin Wall. Struct.*, **156**, 106972. https://doi.org/10.1016/j.tws.2020.106972

Thai, C.H., Ferreira, A.J.M., Tran, T.D. and Phung-Van, P. (2019), "Free vibration, buckling and bending analyses of multilayer functionally graded graphene nanoplatelets reinforced composite plates using the NURBS formulation", *Compos. Struct.*, **220**, 749-759. https://doi.org/10.1016/j.compstruct.2019.03.100

Thai, C.H., Ferreira, A.J.M., Tran, T.D. and Phung-Van, P. (2020), "A size-dependent quasi-3D isogeometric model for functionally graded graphene platelet-reinforced composite microplates based on the modified couple stress theory", *Compos. Struct.*, **234**, 111695. https://doi.org/10.1016/j.compstruct.2019.111695

Thai, H.T., Nguyen, T.K., Vo, T.P., Lee, J. (2014), "Analysis of functionally graded sandwich plates using a new first-order shear deformation theory", *Eur. J. Mech. A Solids*, **45**, 211-225. https://doi.org/10.1016/j.euromechsol.2013.12.008

Torabi, J., Ansari, R., Zabihi, A. and Hosseini, K. (2020), "Dynamic and pull-in instability analyses of functionally graded nanoplates via nonlocal strain gradient theory", *Mech. Based Des. Struct.*, 1-21. https://doi.org/10.1080/15397734.2020.1721298

Wang, Y., Feng, C., Yang, J., Zhou, D. and Liu, W. (2020), "Static response of functionally graded graphene platelet–reinforced composite plate with dielectric property", *J. Intell. Mater. Syst. Struct.*, **31**(19), 2211-2228. https://doi.org/10.1177/1045389X20943955

Xiao, W.S. and Dai, P. (2020), "Static analysis of a circular nanotube made of functionally graded bi-semi-tubes using nonlocal strain gradient theory and a refined shear model", *Eur. J. Mech. A Solids*, 103979. https://doi.org/10.1016/j.euromechsol.2020.103979

Yang, Z., Huang, Y., Liu, A., Fu, J. and Wu, D. (2019), "Nonlinear in-plane buckling of fixed shallow functionally graded graphene reinforced composite arches subjected to mechanical and thermal loading", *Appl. Math. Modell.*, **70**, 315-327. https://doi.org/10.1016/j.apm.2019.01.024

Zhao, S., Zhao, Z., Yang, Z., Ke, L., Kitipornchai, S. and Yang, J. (2020), "Functionally graded graphene reinforced composite structures: A review", *Eng. Struct.*, **210**, 110339. https://doi.org/10.1016/j.engstruct.2020.110339

CC

Appendix

The elements K_{ij}:

$$K_{11} = A_{11}\int_0^a\int_0^b \frac{\partial^3 X_m}{\partial x^3} Y_n \frac{\partial X_m}{\partial x} Y_n \,\mathrm{d}x\mathrm{d}y +$$

$$A_{66}\int_0^a\int_0^b \frac{\partial X_m}{\partial x}\frac{\partial^2 Y_n}{\partial y^2}\frac{\partial X_m}{\partial x} Y_n \,\mathrm{d}x\mathrm{d}y$$

$$K_{12} = (A_{12}+A_{66})\int_0^a\int_0^b \frac{\partial X_m}{\partial x}\frac{\partial^2 Y_n}{\partial y^2}\frac{\partial X_m}{\partial x} Y_n \,\mathrm{d}x\mathrm{d}y$$

$$K_{13} = \left(\frac{A_{11}}{R_x}+\frac{A_{12}}{R_y}\right)\int_0^a\int_0^b \frac{\partial X_m}{\partial x} Y_n \frac{\partial X_m}{\partial x} Y_n \,\mathrm{d}x\mathrm{d}y -$$

$$B_{11}\int_0^a\int_0^b \frac{\partial^3 X_m}{\partial x^3} Y_n \frac{\partial X_m}{\partial x} Y_n \,\mathrm{d}x\mathrm{d}y - (B_{12} +$$

$$2B_{66})\int_0^a\int_0^b \frac{\partial X_m}{\partial x}\frac{\partial^2 Y_n}{\partial y^2}\frac{\partial X_m}{\partial x} Y_n \,\mathrm{d}x\mathrm{d}y$$

$$K_{14} = B_{11}^s\int_0^a\int_0^b \frac{\partial^3 X_m}{\partial x^3} Y_n \frac{\partial X_m}{\partial x} Y_n \,\mathrm{d}x\mathrm{d}y +$$

$$B_{66}^s\int_0^a\int_0^b \frac{\partial X_m}{\partial x}\frac{\partial^2 Y_n}{\partial y^2}\frac{\partial X_m}{\partial x} Y_n \,\mathrm{d}x\mathrm{d}y$$

$$K_{15} = (B_{12}^s+B_{66}^s)\int_0^a\int_0^b \frac{\partial X_m}{\partial x}\frac{\partial^2 Y_n}{\partial y^2}\frac{\partial X_m}{\partial x} Y_n \,\mathrm{d}x\mathrm{d}y$$

$$K_{21} = (A_{12}+A_{66})\int_0^a\int_0^b \frac{\partial^2 X_m}{\partial x^1}\frac{\partial Y_n}{\partial y} X_m \frac{\partial Y_n}{\partial y} \,\mathrm{d}x\mathrm{d}y$$

$$K_{22} = A_{22}\int_0^a\int_0^b X_m \frac{\partial^3 Y_n}{\partial y^3} X_m \frac{\partial Y_n}{\partial y} \,\mathrm{d}x\mathrm{d}y +$$

$$A_{66}\int_0^a\int_0^b\int_0^b \frac{\partial^2 X_m}{\partial x^2}\frac{\partial Y_n}{\partial y} X_m \frac{\partial Y_n}{\partial y} \,\mathrm{d}x\mathrm{d}y$$

$$K_{23} = \left(\frac{A_{12}}{R_x}+\frac{A_{22}}{R_y}\right)\int_0^a\int_0^b X_m \frac{\partial Y_n}{\partial y} X_m \frac{\partial Y_n}{\partial y} \,\mathrm{d}x\mathrm{d}y -$$

$$B_{22}\int_0^a\int_0^b X_m \frac{\partial^3 Y_n}{\partial y^3} X_m \frac{\partial Y_n}{\partial y} \,\mathrm{d}x\mathrm{d}y - (B_{12} +$$

$2B_{66}) \int_0^a \int_0^b \frac{\partial^2 X_m}{\partial x^2} \frac{\partial Y_n}{\partial y} X_m \frac{\partial Y_n}{\partial y} \mathrm{d}x\mathrm{d}y$

$K_{24} = (B_{12}^s + B_{66}^s) \int_0^a \int_0^b \frac{\partial^2 X_m}{\partial x^2} \frac{\partial Y_n}{\partial y} X_m \frac{\partial Y_n}{\partial y} \mathrm{d}x\mathrm{d}y$

$K_{25} = B_{22}^s \int_0^a \int_0^b X_m \frac{\partial^3 Y_n}{\partial y^3} X_m \frac{\partial Y_n}{\partial y} \mathrm{d}x\mathrm{d}y +$

$B_{66}^s \int_0^a \int_0^b \frac{\partial^2 X_m}{\partial x^2} \frac{\partial Y_n}{\partial y} X_m \frac{\partial Y_n}{\partial y} \mathrm{d}x\mathrm{d}y$

$K_{31} = -\left(\frac{A_{11}}{R_x} + \frac{A_{12}}{R_y}\right) \int_0^a \int_0^b \frac{\partial^2 X_n}{\partial x^2} Y_n X_m Y_n \, \mathrm{d}x\mathrm{d}y +$

$B_{11} \int_0^a \int_0^b \frac{\partial^4 X_n}{\partial x^4} Y_n X_m Y_n \, \mathrm{d}x\mathrm{d}y + (B_{12} +$

$2B_{66}) \int_0^a \int_0^b \frac{\partial^2 X_m}{\partial x^2} \frac{\partial^2 Y_n}{\partial y^2} X_m Y_n \, \mathrm{d}x\mathrm{d}y$

$K_{32} = -\left(\frac{A_{12}}{R_x} + \frac{A_{22}}{R_y}\right) \int_0^a \int_0^b X_m \frac{\partial^2 Y_n}{\partial y^2} X_m Y_n \, \mathrm{d}x\mathrm{d}y +$

$B_{22} \int_0^a \int_0^b X_m \frac{\partial^4 Y_n}{\partial y^4} X_m Y_n \, \mathrm{d}x\mathrm{d}y + (B_{12} +$

$2B_{66}) \int_0^a \int_0^b \frac{\partial^2 X_m}{\partial x^2} \frac{\partial^2 Y_n}{\partial y^2} X_m Y_n \, \mathrm{d}x\mathrm{d}y$

$K_{33} = 2\left(\frac{B_{11}}{R_x} + \frac{B_{12}}{R_y}\right) \int_0^a \int_0^b \frac{\partial^2 X_n}{\partial x^2} Y_n X_m Y_n \, \mathrm{d}x\mathrm{d}y + 2\left(\frac{B_{12}}{R_x} +$

$\frac{B_{22}}{R_y}\right) \int_0^a \int_0^b X_m \frac{\partial^2 Y_n}{\partial y^2} X_m Y_n \, \mathrm{d}x\mathrm{d}y - \left(\frac{A_{11}}{{R_x}^2} + 2\frac{A_{12}}{R_x R_y} +$

$\frac{A_{22}}{{R_y}^2}\right) \int_0^a \int_0^b X_m Y_n X_m Y_n \, \mathrm{d}x\mathrm{d}y -$

$D_{11} \int_0^a \int_0^b \frac{\partial^4 X_m}{\partial x^4} Y_n X_m Y_n \, \mathrm{d}x\mathrm{d}y -$

$D_{22} \int_0^a \int_0^b X_m \frac{\partial^4 Y_n}{\partial y^4} X_m Y_n \, \mathrm{d}x\mathrm{d}y - 2(D_{12} +$

$2D_{66}) \int_0^a \int_0^b \frac{\partial^2 X_m}{\partial x^2} \frac{\partial^2 Y_n}{\partial y^2} X_m Y_n \, \mathrm{d}x\mathrm{d}y$

$K_{34} = -\left(\frac{B_{11}^s}{R_x} + \frac{B_{12}^s}{R_y}\right) \int_0^a \int_0^b \frac{\partial^2 X_n}{\partial x^2} Y_n X_m Y_n \, \mathrm{d}x\mathrm{d}y +$

$D_{11}^s \int_0^a \int_0^b \frac{\partial^4 X_m}{\partial x^4} Y_n X_m Y_n \, \mathrm{d}x\mathrm{d}y + (D_{12}^s +$

$2D_{66}^s) \int_0^a \int_0^b \frac{\partial^2 X_m}{\partial x^2} \frac{\partial^2 Y_n}{\partial y^2} X_m Y_n \, \mathrm{d}x\mathrm{d}y$

$K_{35} = -\left(\frac{B_{12}^s}{R_x} + \frac{B_{22}^s}{R_y}\right) \int_0^a \int_0^b X_m \frac{\partial^2 Y_n}{\partial y^2} X_m Y_n \, \mathrm{d}x\mathrm{d}y +$

$D_{22}^s \int_0^a \int_0^b X_m \frac{\partial^4 Y_n}{\partial y^4} X_m Y_n \, \mathrm{d}x\mathrm{d}y \; + (D_{12}^s +$

$2D_{66}^s) \int_0^a \int_0^b \frac{\partial^2 X_m}{\partial x^2} \frac{\partial^2 Y_n}{\partial y^2} X_m Y_n \, \mathrm{d}x\mathrm{d}y$

$K_{41} = B_{11}^s \int_0^a \int_0^b \frac{\partial^3 X_m}{\partial x^3} Y_n \frac{\partial X_m}{\partial x} Y_n \, \mathrm{d}x\mathrm{d}y +$

$B_{66}^s \int_0^a \int_0^b \frac{\partial X_m}{\partial x} \frac{\partial^2 Y_n}{\partial y^2} \frac{\partial X_m}{\partial x} Y_n \, \mathrm{d}x\mathrm{d}y$

$K_{42} = (B_{12}^s + B_{66}^s) \int_0^a \int_0^b \frac{\partial X_m}{\partial x} \frac{\partial^2 Y_n}{\partial y^2} \frac{\partial X_m}{\partial x} Y_n \, \mathrm{d}x\mathrm{d}y$

$K_{43} = \left(\frac{B_{11}^s}{R_x} + \frac{B_{12}^s}{R_y}\right) \int_0^a \int_0^b \frac{\partial X_m}{\partial x} Y_n \frac{\partial X_m}{\partial x} Y_n \, \mathrm{d}x\mathrm{d}y -$

$D_{11}^s \int_0^a \int_0^b \frac{\partial^3 X_m}{\partial x^3} Y_n \frac{\partial X_m}{\partial x} Y_n \, \mathrm{d}x\mathrm{d}y - (D_{12}^s +$

$2D_{66}^s) \int_0^a \int_0^b \frac{\partial X_m}{\partial x} \frac{\partial^2 Y_n}{\partial y^2} \frac{\partial X_m}{\partial x} Y_n \, \mathrm{d}x\mathrm{d}y$

$K_{44} = F_{11}^s \int_0^a \int_0^b \frac{\partial^3 X_m}{\partial x^3} Y_n \frac{\partial X_m}{\partial x} Y_n \, \mathrm{d}x\mathrm{d}y +$

$F_{66}^s \int_0^a \int_0^b \frac{\partial X_m}{\partial x} \frac{\partial^2 Y_n}{\partial y^2} \frac{\partial X_m}{\partial x} Y_n \, \mathrm{d}x\mathrm{d}y -$

$A_{44}^s \int_0^a \int_0^b \frac{\partial X_m}{\partial x} Y_n \frac{\partial X_m}{\partial x} Y_n \, \mathrm{d}x\mathrm{d}y$

$K_{45} = (F_{12}^s + F_{66}^s) \int_0^a \int_0^b \frac{\partial X_m}{\partial x} \frac{\partial^2 Y_n}{\partial y^2} \frac{\partial X_m}{\partial x} Y_n \, \mathrm{d}x\mathrm{d}y$

$K_{51} = (B_{12}^s + B_{66}^s) \int_0^a \int_0^b \frac{\partial^2 X_m}{\partial x^2} \frac{\partial Y_n}{\partial y} X_m \frac{\partial Y_n}{\partial y} \mathrm{d}x\mathrm{d}y$

$K_{52} = B_{22}^s \int_0^a \int_0^b X_m \frac{\partial^3 Y_n}{\partial y^3} X_m \frac{\partial Y_n}{\partial y} \mathrm{d}x\mathrm{d}y +$

$B_{66}^s \int_0^a \int_0^b \frac{\partial^2 X_m}{\partial x^2} \frac{\partial Y_n}{\partial y} X_m \frac{\partial Y_n}{\partial y} \mathrm{d}x\mathrm{d}y$

$K_{53} = \left(\frac{B_{12}^s}{R_x} + \frac{B_{22}^s}{R_y}\right) \int_0^a \int_0^b X_m \frac{\partial Y_n}{\partial y} X_m \frac{\partial Y_n}{\partial y} \mathrm{d}x\mathrm{d}y -$

$D_{22}^s \int_0^a \int_0^b X_m \frac{\partial^3 Y_n}{\partial y^3} X_m \frac{\partial Y_n}{\partial y} \mathrm{d}x\mathrm{d}y - (D_{12}^s +$

$2D_{66}^s) \int_0^a \int_0^b \frac{\partial^2 X_m}{\partial x^2} \frac{\partial Y_n}{\partial y} X_m \frac{\partial Y_n}{\partial y} \mathrm{d}x\mathrm{d}y$

$K_{54} = (F_{12}^s + F_{66}^s) \int_0^a \int_0^b \frac{\partial^2 X_m}{\partial x^2} \frac{\partial Y_n}{\partial y} X_m \frac{\partial Y_n}{\partial y} \mathrm{d}x\mathrm{d}y$

$K_{55} = F_{22}^s \int_0^a \int_0^b X_m \frac{\partial^3 Y_n}{\partial y^3} X_m \frac{\partial Y_n}{\partial y} \mathrm{d}x\mathrm{d}y +$

$F_{66}^s \int_0^a \int_0^b \frac{\partial^2 X_m}{\partial x^2} \frac{\partial Y_n}{\partial y} X_m \frac{\partial Y_n}{\partial y} \mathrm{d}x\mathrm{d}y -$

$A_{55}^s \int_0^a \int_0^b X_m \frac{\partial Y_n}{\partial y} X_m \frac{\partial Y_n}{\partial y} \mathrm{d}x\mathrm{d}y$

Mass matrix elements;

$M_{11} = I_0 \int_0^a \int_0^b \frac{\partial X_m}{\partial x} Y_n \frac{\partial X_m}{\partial x} Y_n \, \mathrm{d}x\mathrm{d}y$

$M_{13} = -I_1 \int_0^a \int_0^b \frac{\partial X_m}{\partial x} Y_n \frac{\partial X_m}{\partial x} Y_n \, \mathrm{d}x\mathrm{d}y$

$M_{14} = I_3 \int_0^a \int_0^b \frac{\partial X_m}{\partial x} Y_n \frac{\partial X_m}{\partial x} Y_n \, \mathrm{d}x\mathrm{d}y$

$M_{22} = I_0 \int_0^a \int_0^b X_m \frac{\partial Y_n}{\partial y} X_m \frac{\partial Y_n}{\partial y} \mathrm{d}x\mathrm{d}y$

$M_{23} = -I_1 \int_0^a \int_0^b X_m \frac{\partial Y_n}{\partial y} X_m \frac{\partial Y_n}{\partial y} \mathrm{d}x\mathrm{d}y$

$M_{25} = -I_3 \int_0^a \int_0^b X_m \frac{\partial Y_n}{\partial y} X_m \frac{\partial Y_n}{\partial y} \mathrm{d}x\mathrm{d}y$

$M_{31} = I_1 \int_0^a \int_0^b \frac{\partial^2 X_m}{\partial x^2} Y_n X_m Y_n \, \mathrm{d}x\mathrm{d}y$

$M_{32} = I_1 \int_0^a \int_0^b X_m \frac{\partial^2 Y_n}{\partial y^2} X_m Y_n \, \mathrm{d}x\mathrm{d}y$

$M_{33} = I_0 \int_0^a \int_0^b X_m Y_n X_m Y_n \, \mathrm{d}x\mathrm{d}y -$

$I_2 \left(\int_0^a \int_0^b \frac{\partial^2 X_m}{\partial x^2} Y_n X_m Y_n \, \mathrm{d}x\mathrm{d}y + \int_0^a \int_0^b X_m \frac{\partial^2 Y_n}{\partial y^2} X_m Y_n \, \mathrm{d}x\mathrm{d}y\right)$

$M_{34} = -I_4 \int_0^a \int_0^b \frac{\partial^2 X_m}{\partial x^2} Y_n X_m Y_n \, \mathrm{d}x\mathrm{d}y$

$M_{34} = -I_4 \int_0^a \int_0^b X_m \frac{\partial^2 Y_n}{\partial y^2} X_m Y_n \, \mathrm{d}x\mathrm{d}y$

$M_{41} = I_3 \int_0^a \int_0^b \frac{\partial X_m}{\partial x} Y_n \frac{\partial X_m}{\partial x} Y_n \, \mathrm{d}x\mathrm{d}y$

$M_{43} = -I_4 \int_0^a \int_0^b \frac{\partial X_m}{\partial x} Y_n \frac{\partial X_m}{\partial x} Y_n \, \mathrm{d}x\mathrm{d}y$

$M_{44} = I_5 \int_0^a \int_0^b \frac{\partial X_m}{\partial x} Y_n \frac{\partial X_m}{\partial x} Y_n \, \mathrm{d}x\mathrm{d}y$

$M_{52} = I_3 \int_0^a \int_0^b X_m \frac{\partial Y_n}{\partial y} X_m \frac{\partial Y_n}{\partial y} \mathrm{d}x\mathrm{d}y$

$M_{53} = -I_4 \int_0^a \int_0^b X_m \frac{\partial Y_n}{\partial y} X_m \frac{\partial Y_n}{\partial y} \mathrm{d}x\mathrm{d}y$

$M_{55} = -I_5 \int_0^a \int_0^b X_m \frac{\partial Y_n}{\partial y} X_m \frac{\partial Y_n}{\partial y} \mathrm{d}x\mathrm{d}y$

$M_{12} = M_{15} = M_{21} = M_{24} = M_{42} = M_{45} = M_{51} = M_{54} = 0$